

Evaluation of the N₂O rate of change to understand the stratospheric Brewer-Dobson Circulation in a Chemistry-Climate Model

Daniele Minganti¹, Simon Chabrillat¹, Quentin Errera¹, Maxime Prignon^{2*}, Douglas E. Kinnison³, Rolando R. Garcia³, Marta Abalos⁴, Justin Alsing^{5,9}, Matthias Schneider⁶, Dan Smale⁷, Nicholas Jones⁸, Emmanuel Mahieu²

¹Royal Belgian Institute for Space Aeronomy, BIRA-IASB, Brussels, Belgium

²Institute of Astrophysics and Geophysics, UR SPHERES, University of Liège, Liège, Belgium

³National Center for Atmospheric Research, Boulder, CO, USA

⁴Universidad Complutense de Madrid, Madrid, Spain

⁵Oskar Klein Centre for Cosmoparticle Physics, Department of Physics, Stockholm University, Stockholm

SE-106 91, Sweden

⁶Institute of Meteorology and Climate Research (IMK-ASF), Karlsruhe Institute of Technology,

Karlsruhe, Germany

⁷National Institute of Water and Atmospheric Research, Lauder, New Zealand

⁸School of Chemistry, University of Wollongong, Wollongong, Australia

⁹Imperial Centre for Inference and Cosmology, Department of Physics, Imperial College London, Blackett

Laboratory, Prince Consort Road, London SW7 2AZ, UK

Key Points:

- Sparse sampling of Atmospheric Chemistry Experiment Fourier Transform Spectrometer exaggerates the stratospheric nitrous oxide trends
- Transformed Eulerian Mean analysis shows that the residual mean advection contributes to the positive nitrous oxide trend in the Tropics
- The Whole Atmosphere Community-Climate Model simulates weaker hemispheric asymmetries of the nitrous oxide trends compared to reanalyses

*Currently at: Department of Earth, Space and Environment, Chalmers University of Technology, 41296, Gothenburg, Sweden

Corresponding author: Daniele Minganti, daniele.minganti@aeronomie.be

Abstract

The Brewer-Dobson Circulation (BDC) determines the distribution of long-lived tracers in the stratosphere; therefore, their changes can be used to diagnose changes in the BDC. We evaluate decadal (2005-2018) trends of nitrous oxide (N_2O) in two versions of the Whole Atmosphere Chemistry-Climate Model (WACCM) by comparing them with measurements from four Fourier transform infrared (FTIR) ground-based instruments, the Atmospheric Chemistry Experiment Fourier Transform Spectrometer (ACE-FTS), and with a chemistry-transport model (CTM) driven by four different reanalyses. The limited sensitivity of the FTIR instruments can hide negative N_2O trends in the mid-stratosphere because of the large increase in the lowermost stratosphere. When applying ACE-FTS measurement sampling on model datasets, the reanalyses from the European Centre for Medium Range Weather Forecast (ECMWF) compare best with ACE-FTS, but the N_2O trends are consistently exaggerated. The N_2O trends obtained with WACCM disagree with those obtained from ACE-FTS, but the new WACCM version performs better than the previous above the Southern Hemisphere in the stratosphere. Model sensitivity tests show that the decadal N_2O trends reflect changes in the stratospheric transport. We further investigate the N_2O Transformed Eulerian Mean (TEM) budget in WACCM and in the CTM simulation driven by the latest ECMWF reanalysis. The TEM analysis shows that enhanced advection affects the stratospheric N_2O trends in the Tropics. While no ideal observational dataset currently exists, this model study of N_2O trends still provides new insights about the BDC and its changes because of the contribution from relevant sensitivity tests and the TEM analysis.

Plain Language Summary

The circulation in the stratosphere is characterized by upward motion above the Tropics, followed by poleward and downward motions above the high latitudes. Changes in the pattern of this stratospheric circulation are currently a challenging topic of research. We investigate the decennial changes of this stratospheric circulation using observations and numerical simulations of the long-lived tracer nitrous oxide. Observations are obtained from ground-based and satellite instruments. Numerical simulations include complex atmospheric models that reproduce the chemistry and dynamics of the stratosphere. Both observations and models show differences between the hemispheres in the nitrous oxide decennial changes. Unfortunately, the current observations of nitrous oxide are not perfect. The ground-based instruments cannot correctly measure the changes of nitrous oxide in the northern hemisphere. The satellite does not measure at all times, and it spatially covers more the high latitudes, which negatively affects the measurements of nitrous oxide. On the other hand, model simulations can provide valuable insights into the changes in the stratospheric circulation. They show that changes in the stratospheric circulation cause the differences between hemispheres in the nitrous oxide trends and show that the circulation changes can be associated with different physical processes.

1 Introduction

Nitrous oxide (N_2O) is continuously emitted in the troposphere, with a nearly constant rate of change of 2% per decade, and transported into the stratosphere, where it is destroyed by photodissociation mainly in the Tropics above 35 km (Tian et al., 2020). The atmospheric lifetime of N_2O is approximately 120 years, which makes it an excellent tracer for stratospheric transport studies (Seinfeld & Pandis, 2016). Within the stratosphere, the lifetime of N_2O depends also on the solar activity because of its influence on the photolysis rates, with slightly decreased lifetime during solar maxima and increased lifetime during solar minima (Prather et al., 2015).

N_2O enters the stratosphere in the Tropics, and is transported towards higher latitudes by the Brewer-Dobson Circulation (BDC, Dobson et al., 1929; Brewer, 1949; Dob-

76 son, 1956). The BDC is driven by the breaking of tropospheric waves that propagate into
77 the stratosphere (e.g., Charney & Drazin, 1961) and is often separated into an advective
78 component, the residual mean meridional circulation (hereafter residual circulation),
79 and a mixing component (Garny et al., 2014). The residual circulation consists in up-
80 welling in the Tropics, followed by poleward flow and downwelling over the middle and
81 high latitudes (Plumb, 2002). The mixing is a two-way exchange of mass that, within
82 the stratosphere, occurs mostly on isentropic surfaces, thus, it is mainly quasi-horizontal
83 (Shepherd, 2007). The BDC has a significant impact in determining the stratospheric
84 distribution of chemical tracers, like ozone and greenhouse gases (e.g., Butchart, 2014),
85 and in maintaining the observed meridional and vertical temperature structure of the strato-
86 sphere (Holton, 2004). Long-term changes in the BDC can have significant impacts on
87 the climate system. One of the most important is the effect on the recovery of strato-
88 spheric ozone, as a changing BDC would result in changes of its meridional distribution
89 (e.g., Shepherd, 2008; Dhomse et al., 2018). Changes in the BDC also impact the life-
90 time of Ozone Depleting Substances (ODS) in the stratosphere (Butchart & Scaife, 2001;
91 Waugh & Hall, 2002), as well as the water vapor entering the stratosphere through the
92 Tropics (e.g., Randel & Park, 2019). The troposphere is also affected by BDC changes
93 because of the impact on the mass exchange with the stratosphere (e.g., ozone, Meul et
94 al., 2018), and on the ultra-violet radiation reaching the surface (Meul et al., 2016).

95 Given the relevance of the BDC changes, understanding them is thus fundamen-
96 tal to fully comprehend the past and future evolution of climate. Simulations by Chemistry-
97 Climate Models (CCMs) robustly project an acceleration of the BDC throughout the strato-
98 sphere in recent and coming decades due to the increase of greenhouse gases (e.g., Aba-
99 los et al., 2021). On the other hand, Oberländer-Hayn et al. (2016) argue that the global
100 BDC trends in the lower stratosphere in CCMs are caused to a large extent by a lift of
101 the tropopause level in response to global warming rather than an actual speedup of the
102 circulation. Another significant impact of the increase of greenhouse gases is the shrink-
103 age of the stratosphere, i.e., the combination of the tropopause rise and the downward
104 shift of the height of the pressure levels above 55 km, that results from its cooling over
105 the last decades (Pisoft et al., 2021). Modelling studies have shown that this stratospheric
106 shrinking can impact the BDC and modulate its changes over the past decades (Šácha
107 et al., 2019; Eichinger & Šácha, 2020). Such modulation consists in a BDC acceleration
108 similar to that resulting from the impact of the tropopause lift (Eichinger & Šácha, 2020).
109 In addition, CCMs simulations show that also the vertical and meridional structure of
110 the BDC has changed in the past decades in response to climate change (Hardiman et
111 al., 2014). Other modeling studies have shown that mixing, both on resolved and un-
112 resolved scales, also plays an important role in the simulated magnitudes of the BDC
113 changes in addition to changes in the residual circulation among CCMs (e.g., Eichinger
114 et al., 2019). Recent studies have also shown that ODS, through their impact on ozone,
115 play a significant role in the modeled BDC changes (Abalos et al., 2019). In particular,
116 the ODS decrease resulting from the Montreal Protocol, will reduce the global warming-
117 induced acceleration of the BDC and potentially lead to hemispheric asymmetries in the
118 BDC trends (Polvani et al., 2019).

119 The BDC and its changes cannot be measured directly (e.g., Minschwaner et al.,
120 2016), but can be indirectly examined from measurements of stratospheric long-lived trac-
121 ers (e.g., Engel et al., 2009; Hegglin et al., 2014) or temperature (Fu et al., 2015). Re-
122 cently, Strahan et al. (2020) used ground-based observations of nitric acid and hydro-
123 gen chloride to investigate hemispheric-dependent BDC changes in the stratosphere. Sim-
124 ilarly, space-borne observations of stratospheric tracers are often used to investigate decadal
125 changes in the BDC using, e.g., hydrogen fluoride (Harrison et al., 2016), ozone (Nedoluha
126 et al., 2015) or N₂O (Han et al., 2019). Measurements of stratospheric tracers are often
127 used to calculate the mean Age of Air (AoA, Hall & Plumb, 1994). The mean AoA is
128 a widely used diagnostic for stratospheric transport and is defined as the transit time
129 of an air parcel from the tropical tropopause (or the surface, depending on the defini-

tion) to a certain point of the stratosphere (Vaugh & Hall, 2002). Engel et al. (2017) used balloon-borne observations of carbon dioxide and methane to derive mean AoA trends above the northern mid-latitudes in the mid-lower stratosphere. Engel et al. (2017) found positive but not statistically significant mean AoA trends over about 40 years (corresponding to a possible slowdown of the BDC), which is in contrast with the modeling studies that simulate a significant acceleration of the BDC over the same region (e.g., Abalos et al., 2021). These discrepancies can be partly attributed to the temporal and spatial sparseness of the measurements and to uncertainties in the mean AoA trends derived from real tracers (Garcia et al., 2011; Fritsch et al., 2020). In addition to ground-based measurements, space-borne observations have been used to compute mean AoA trends as well (e.g., Stiller et al., 2012; Haenel et al., 2015). These observational studies using remote sensing measurements have shown a hemispheric asymmetry in the mean AoA trends over 2002-2012, with positive changes in the Northern Hemisphere (NH) and negative changes in the Southern Hemisphere (SH) (e.g., Mahieu et al., 2014; Stiller et al., 2017). The mean AoA indirectly obtained from satellite measurements in these studies does not allow the separation between residual circulation and mixing, which was proven to be important in CCMs (Dietmüller et al., 2018). However, Linz et al. (2021) showed that the effect of mixing can be explicitly calculated using AoA vertical gradients from both models and satellite measurements. In addition, von Clarmann and Grabowski (2021) (similarly to the early study of Holton & Choi, 1988) proposed an alternative method to infer the stratospheric circulation from satellite measurements of long-lived tracers by a direct inversion of the continuity equation.

Reanalysis datasets try to fill the gap between observations and free-running models, providing a global multi-decadal and continuous state of the past atmosphere by assimilating available observations. Dynamical fields from reanalyses can be used to drive Chemistry-Transport Models (CTMs) to simulate the distribution of real and synthetic tracers in the atmosphere. In the past decade, these CTM experiments have been used to investigate BDC changes in reanalyses using the AoA diagnostic (e.g., Monge-Sanz et al., 2012; Diallo et al., 2012; Ploeger et al., 2015). However, significant differences exist in the BDC changes obtained from different reanalyses, both over multi-decadal and decadal time scales (e.g., Abalos et al., 2015; Chabrilat et al., 2018). Furthermore, the computation of mean AoA largely depends on whether the kinematic velocities or the heating rates are used to drive the CTMs, leading to significant differences within the same reanalysis (Ploeger et al., 2019).

This study is based on the work performed by Minganti et al. (2020, hereafter M2020), who evaluated the climatological BDC in the Whole Atmosphere Community Climate Model (WACCM) version 4 (Garcia et al., 2017). The evaluation in M2020 consisted in studying the impact of the BDC on the climatologies of the stratospheric N_2O abundances and of the N_2O Transformed Eulerian Mean (TEM) budget (Andrews et al., 1987). This evaluation was performed by comparison with simulations of the Belgian Assimilation System for Chemical Observation Chemistry-Transport Model CTM (BASCOE CTM, Chabrilat et al., 2018) driven by dynamical reanalyses and with the BASCOE reanalysis of Aura Microwave Limb Sounder (MLS) version 2 (BRAM2, Errera et al., 2019). The TEM diagnostic was included in M2020 because it allows separating the effects of transport and chemistry on the rate of change of a stratospheric tracer such as N_2O (Randel et al., 1994). Within the TEM framework, the impact of transport can be further separated into the impact from the residual circulation and mixing, as was done for ozone and carbon monoxide in Abalos et al. (2013). It is important to note that the mixing obtained from the TEM analysis generally includes contributions from advective transport that are not represented by the residual circulation (Holton, 2004). After studying the climatologies in M2020, the present study aims to evaluate the changing BDC in WACCM in its versions 4 and 6 (Gettelman et al., 2019) by studying multi-decadal and decadal changes of N_2O in the stratosphere, comparing them with ground-based and space-borne observations and BASCOE CTM simulations. We also evaluate the changes

184 in TEM N₂O budget in WACCM and in the BASCOE CTM. We compare the model
 185 simulations with ground-based observations of N₂O from Fourier transform infrared (FTIR)
 186 spectrometers that are part of the Network for the Detection of Atmospheric Compo-
 187 sition Change (NDACC) at four stations in the SH and NH subtropics as well as at mid-
 188 latitudes (De Mazière et al., 2018, <http://www.ndaccdemo.org/>). We also use satellite
 189 measurements from the Atmospheric Chemistry Experiment Fourier Transform Spec-
 190 trometer (ACE-FTS, Bernath et al., 2021). Contrary to M2020, we cannot use N₂O from
 191 BRAM2 because of the unrealistic negative drift in the MLS N₂O dataset (Livesey et
 192 al., 2021). The BASCOE CTM is driven by four modern reanalyses that are part of the
 193 SPARC (Stratosphere-troposphere Processes and their Role in Climate) Reanalysis In-
 194 tercomparison Project (S-RIP, Fujiwara et al., 2017).

195 The present study is structured as follows. Section 2 describes the observational
 196 and modeling datasets used in this study, as well as the TEM diagnostics and the regres-
 197 sion model used to derive linear trends. In Section 3, we use FTIR observations to eval-
 198 uate the trends in the stratospheric N₂O columns obtained from WACCM and the CTM
 199 simulations and from satellite measurements. In Section 4, using ACE-FTS as a refer-
 200 ence, we study the global N₂O trends in the stratosphere and focus on the differences
 201 in the trend patterns among datasets. In Section 5, we investigate the N₂O TEM bud-
 202 get from WACCM version 6 and a BASCOE simulation in order to separate the impact
 203 of the residual circulation and mixing on the N₂O trends. Finally, Section 6 concludes
 204 the study with a summary of the principal findings.

205 2 Data and Methods

206 This section describes the observational and model data as well as the methods used
 207 in this study (see Tables 1 and 2). Throughout the study, we will refer to the CCMs and
 208 the BASCOE CTM simulations as "models" to distinguish them from the observations
 209 obtained from the FTIR and ACE-FTS. For the sake of brevity, we refer to M2020 for
 210 a more detailed description of the dataset (BASCOE CTM, WACCM version 4, and S-
 RIP reanalyses) and methods (TEM framework) already used there.

Dataset name	Full Name	Reference	Year range	Vert. resol. + top
WACCM-REFC1	Whole Atmosphere Commu- nity Climate Model	Marsh et al. (2013) Garcia et al. (2017)	1985-2018	L66, 5.96 10 ⁻⁶ hPa
WACCM-REFD1	Whole Atmosphere Commu- nity Climate Model	Gettelman et al. (2019)	1985-2018	L70, 5.96 10 ⁻⁶ hPa
CTM+ERA1	ECMWF Reanalysis Interim	Dee et al. (2011)	1985-2018	L60, 0.1 hPa
CTM+ERA5	ECMWF Reanalysis 5	Hersbach et al. (2020)	1985-2019	L86, 0.01 hPa
CTM+JRA55	Japanese 55-year Reanalysis	Kobayashi et al. (2015)	1985-2018	L60, 0.2 hPa
CTM+MERRA2	Modern-Era Retrospective analysis for Research and Applications	Gelaro et al. (2017)	1985-2018	L72, 0.01 hPa
ACE-FTS	Atmospheric Chemistry Ex- periment Fourier Transform Spectrometer	Bernath et al. (2021)	2005-present	L42, 150 km

Table 1. Overview of the models and satellite measurements used in this study.

Station name	Reference	Location (lat and lon)	Altitude	strato DOFS
Lauder	Zhou et al. (2019)	45.4°S and 169.68°E	370 m	2
Wollongong	Griffith et al. (2012)	34.45°S and 150.88°E	30 m	2
Izaña	García et al. (2021)	28.30°N and 16.48°E	2367 m	1.5
Jungfraujoch	Zander et al. (2008)	46.55°N and 7.98°E	3580 m	1.1

Table 2. Overview of FTIR stations considered in this study.

2.1 Ground-based FTIR Observations

We use ground-based measurements of stratospheric N₂O columns obtained at four stations that are part of NDACC: Lauder (New Zealand, 45°S), Wollongong (Australia, 34°S), Izaña (Spain, 28°N) and Jungfraujoch (Switzerland, 46°N) (Zhou et al., 2019). The solar absorption spectra under clear-sky conditions with the ground-based FTIR measurements taken under the auspices of the NDACC allow the acquisition of long-term consistent data sets. The stations have been chosen at the mid-latitudes and subtropics where the observed BDC changes are the largest (e.g., Strahan et al., 2020).

At Jungfraujoch, measurements have been obtained from two spectrometers: an instrument developed at the University of Liège (1984-2008), and a Bruker IFS 120HR (early 1990's-present) (Zander et al., 2008; Prignon et al., 2019). In this study, we use the spectra taken by the Bruker spectrometer to investigate the most recent period. Ground-based measurements of N₂O profiles at Lauder started in 2001 with a Bruker 120HR spectrometer, replaced in 2018 (with 6 months overlap) by a Bruker 125HR (Strong et al., 2008; Zhou et al., 2019). The Lauder station is particularly relevant as is the only FTIR site of NDACC located in the SH mid-latitudes. The Wollongong station has provided data for the SH subtropics since 1996. Solar spectra were measured with a Bomem instrument until 2007, which was then replaced by a Bruker 125HR (Griffith et al., 2012). N₂O profiles are also measured at the Izaña Observatory since 1999. This high-altitude station is characterized by excellent conditions for FTIR spectroscopy, with clear sky conditions for most of the year. Observations started using a Bruker 120M spectrometer and continued, since 2005, with a Bruker 125HR (García et al., 2021). The retrieval code for the N₂O profiles is the SFIT-v4 (v0.9.4.4) for the Jungfraujoch, Lauder and Wollongong stations, and PROFITT9 for the Izaña station (Zhou et al., 2019).

We consider stratospheric N₂O columns between 12 and 40 km of altitude because the instruments at all stations are the most sensitive to the measured N₂O profiles over this stratospheric region (not shown). The degrees of freedom for signal (DOFS), which quantify the vertical resolution of the measurement (Rodgers, 2000), vary largely between the stations. For N₂O, the stratospheric DOFS between 12 and 40 km of the instruments in the SH are approximately 2, allowing the separation of two layers within the stratosphere. On the other hand, the stratospheric DOFS of the instruments in the NH are around 1.5 for Izaña, and 1 for Jungfraujoch, limiting the analysis to one stratospheric layer between 12 and 40 km. Thus, in order to perform a fair comparison, we compute one stratospheric N₂O column between 12 and 40 km for all stations. In order to take into account the limited sensitivity of the FTIR measurements, we smooth the ACE-FTS data and the model output on the FTIR vertical grid using the FTIR averaging kernels as described in Langerock et al. (2015).

249

2.2 Spaceborne Measurements - ACE-FTS

250

251

252

253

254

255

ACE-FTS, onboard the SCISAT Canadian satellite, was launched in August 2003 on a high inclination (74°) low earth orbit (650 km) and is still in operation in 2022 (Bernath et al., 2005; Bernath, 2017). The ACE-FTS instrument measures the infrared absorptions from solar occultations between 2.2 and $13.3 \mu\text{m}$ with a spectral resolution of 0.02 cm^{-1} . This allows the retrieval of vertically resolved mixing ratio profiles for 44 molecules and 24 isotopologues from each measurement (Bernath et al., 2020).

256

257

258

259

260

261

262

263

264

In this study, we use version 4.1 of the ACE-FTS data. It differs from previous versions by the significantly better retrievals at low altitudes and led to substantially improved trends compared to the earlier version 3.5 (Bernath et al., 2021). For N_2O , previous comparisons of v3.6 with independent satellite instruments showed a good agreement below 35 km (within 10%) and larger biases above that level (within 20%, Sheese et al., 2017). In our study, N_2O profiles are filtered for outliers using the method described in Sheese et al. (2017) and are then vertically regridded to a constant pressure vertical grid using a mass-conservative scheme (Bader et al., 2017). For trend analysis, profiles are monthly averaged on latitude bins with 5° spacing from pole to pole.

265

266

267

268

269

270

271

272

273

In order to compare the trend analysis of model simulations with those obtained by ACE-FTS, the model datasets are first re-sampled from their native temporal and spatial grids (model space) to match those of ACE-FTS (observational space). This is important in particular due to the low sampling of ACE-FTS - only 30 daily profiles due to the solar occultation method. The re-sampling is done by finding model output adjacent in time to each ACE-FTS profile (BASCOE and WACCM datasets used in this study have, respectively, 6 hourly and daily output) and then by linearly interpolating the model values in time and space at the profile geolocation. The re-sampled model datasets are then averaged over a month as done with ACE-FTS.

274

2.3 BASCOE CTM and Driving Reanalyses

275

276

277

278

279

280

281

282

283

In this study, we use the BASCOE CTM driven by four dynamical reanalyses: the European Centre for Medium-Range Weather Forecast Interim reanalysis (ERA-I, Dee et al., 2011), and its newer version ERA5 (Hersbach et al., 2020), the Modern-Era Retrospective analysis for Research and Applications version 2 (MERRA2, Gelaro et al., 2017), and the Japanese 55-year Reanalysis (JRA55, Kobayashi et al., 2015). In the following, we provide a brief overview of the BASCOE CTM and the ERA-I, MERRA2 and JRA55 reanalyses, as more detailed information can be found in such companion studies: Chabrillat et al. (2018); Prignon et al. (2019, 2021) and M2020. Since ERA5 is not detailed in these publications, we provide a more detailed description.

284

285

286

287

288

289

290

291

292

293

294

The BASCOE CTM is built on a kinematic transport module (that takes as input the surface pressure and the horizontal winds) with a flux-form semi-Lagrangian (FFSL) advection scheme (Lin & Rood, 1996). The FFSL scheme is run on a common horizontal grid of $2^\circ \times 2.5^\circ$ for all the reanalyses, while the vertical grid depends on the input reanalysis. The chemical scheme explicitly solves for stratospheric chemistry, and includes 65 chemical species and 243 reactions (Prignon et al., 2019). ERA-I and JRA55 have 60 levels up to 0.1 hPa, MERRA2 has 72 levels up to 0.01 hPa. The model setup, as well as the boundary conditions (including those for N_2O), are the ones used in Prignon et al. (2019), M2020 and Prignon et al. (2021). Readers are directed towards Chabrillat et al. (2018) for a detailed description of the BASCOE CTM and its driving by the ERA-I, JRA55 and MERRA2 reanalyses.

295

296

297

298

The ERA5 reanalysis is the fifth generation of reanalysis produced by the ECMWF and covers the 1979-present period, with a programmed extension back to 1950 (Hersbach et al., 2020). The horizontal resolution is 31 km, with hourly output frequency, and the vertical grid ranges from the surface to 0.01 hPa with 137 levels and with 300-600 m ver-

299 tical spacing in the troposphere and stratosphere, which increases to 1-3 km above 30
 300 km. ERA5 suffers from a cold bias in the lower stratosphere from 2000 to 2006. For this
 301 reason, a new analysis (ERA5.1) has been produced for that period to correct for that
 302 bias (Simmons et al., 2020). In this study, the BASCOE CTM was driven by ERA5.1
 303 for the 2000-2006 period. For computational reasons, the vertical resolution is reduced
 304 to 86 levels from the original 137 keeping the original vertical spacing in the stratosphere,
 305 and we used 6-hourly (0000, 0600, 1200, 1800 UTC) data. As done for the other reanal-
 306 yses, the ERA5 data on the fine 31-km grid were truncated at wavenumber 47 to avoid
 307 aliasing on the target $2.5^\circ \times 2^\circ$ horizontal grid (Chabrillat et al., 2018).

308 In order to further investigate the contribution of transport in ERA5, we performed
 309 two sensitivity tests with the BASCOE CTM driven by that reanalysis. To isolate the
 310 contribution of transport, the first sensitivity test consists of a fixed N_2O run, i.e., a BAS-
 311 COE CTM simulation where N_2O does not increase over time. We accomplished that
 312 by performing a BASCOE CTM run exactly as the ERA5 simulation but keeping the
 313 N_2O volume mixing ratios at the surface fixed to their values at the beginning of the sim-
 314 ulation (cst- N_2O). Any N_2O trend for the cst- N_2O simulation is therefore due only to
 315 the effect of transport. The second sensitivity test is a perpetual year simulation that
 316 is complementary to cst- N_2O , and consists of an experiment where the transport does
 317 not change over time (cst-dyn). In order to include a complete Quasi Biennial Oscilla-
 318 tion cycle (QBO, Baldwin et al., 2001), we used the years 2006 and 2007 from ERA5.1
 319 and ERA5, respectively. Those years are unusual (but convenient) because the QBO lasted
 320 exactly 24 months (see the zonal wind data at Singapore [https://www.geo.fu-berlin](https://www.geo.fu-berlin.de/met/ag/strat/produkte/qbo/singapore.dat)
 321 [.de/met/ag/strat/produkte/qbo/singapore.dat](https://www.geo.fu-berlin.de/met/ag/strat/produkte/qbo/singapore.dat)). We used the dynamics of the year
 322 2006 to simulate even years and from the year 2007 for odd years. All the N_2O changes
 323 simulated by cst-dyn are due to its constant increase at the surface.

324 2.4 WACCM

325 In this study, we use two versions of WACCM: version 4 (Marsh et al., 2013; Gar-
 326 cia et al., 2017) and version 6 (Gettelman et al., 2019). WACCM version 4 (WACCM4)
 327 is the atmospheric component of the Community Earth System Model version 1.2.2 (CESM,
 328 Hurrell et al., 2013), which has been developed by the U.S. National Center of Atmo-
 329 spheric Research. It is the extended (whole atmosphere) version of the Community At-
 330 mosphere Model version 4 (CAM4, Neale et al., 2013). WACCM4 has a longitude-latitude
 331 grid of $2.5^\circ \times 1.9^\circ$ and 66 vertical levels from the surface to about 140 km altitude, with
 332 1.1-1.75 km vertical spacing in the stratosphere. The physics of WACCM4 is the same
 333 as CAM4 and the dynamical core is a finite volume with a horizontal discretization based
 334 on a conservative flux-form semi Lagrangian (FFSL) scheme (Lin, 2004). WACCM4 is
 335 not able to internally generate the QBO; thus, it is nudged towards observations of strato-
 336 spheric winds (Matthes et al., 2010). In this study, we use the WACCM4 version included
 337 within the SPARC (Stratosphere-troposphere Processes And their Role in Climate) Chemistry-
 338 Climate Model Intercomparison phase 1 (CCMI-1, Morgenstern et al., 2017). In partic-
 339 ular, we use the REFC1 experiments (WACCM-REFC1), which consist of simulations
 340 of the recent past (1960-2018) using state-of-the-art historical forcings and observed sea-
 341 surface temperatures (Morgenstern et al., 2017). For N_2O , the boundary conditions are
 342 prescribed using the forcing recommended by the CCMI (Eyring et al., 2013). Compared
 343 to the default WACCM4 version, WACCM-REFC1 includes important modifications of
 344 the treatment of heterogeneous chemistry and of the gravity waves parameterization, which
 345 ultimately improve the simulation of ozone in the Southern Hemisphere (Garcia et al.,
 346 2017). In this study, we use three realizations of the WACCM-REFC1 configuration for
 347 the 1985-2018 period.

348 Version 6 of WACCM (WACCM6) is the extension to the whole atmosphere of ver-
 349 sion 6 of CAM that is part of version 2 of CESM (Danabasoglu et al., 2020). The de-
 350 fault horizontal resolution of WACCM6 is $0.9^\circ \times 1.25^\circ$ latitude-longitude, with 70 levels

351 in the vertical from the ground to around 140 km, with vertical resolution similar to WACCM4.
 352 The transition from WACCM4 to WACCM6 involved several changes in the physics and
 353 chemistry that are described in Gettelman et al. (2019). WACCM6 is part of the Cou-
 354 pled Model Intercomparison Project Phase 6 (CMIP6, Eyring et al., 2016), and is used
 355 in the CCMI-2022 activity (i.e., the successor of CCMI-1, Plummer et al., 2021). Within
 356 CCMI-2022, we use the REFD1 WACCM6 experiments (WACCM-REFD1), i.e., a suite
 357 of hindcast experiments for the recent past (1960-2018) used to compare with observa-
 358 tions. The REFD1 experiments use the databases for historical forcings and observed
 359 sea surface temperatures developed for the CMIP6. The N₂O emissions are specified fol-
 360 lowing the CMIP6 recommendation for historical simulations, i.e., following Meinshausen
 361 et al. (2020). Although WACCM6 can internally produce the QBO, the REFD1 exper-
 362 iments require a nudged QBO towards observed winds to ensure synchronization with
 363 historical variability. In this study, we use one realization of the WACCM-REFD1 ex-
 364 periments for the 1985-2018 period.

365 2.5 TEM Diagnostics

For stratospheric tracers, the TEM diagnostics (Andrews et al., 1987) allows sep-
 arating the impact of transport and chemistry on the zonal mean local rate of change
 of a tracer with mixing ratio χ :

$$\bar{\chi}_t = -v^* \bar{\chi}_y - w^* \bar{\chi}_z + e^{z/H} \nabla \cdot \mathbf{M} + \bar{S} + \bar{\epsilon}, \quad (1)$$

366 where χ represents N₂O, $\mathbf{M} = -e^{-z/H} (\overline{v'\chi'} - \overline{v'\theta'} \bar{\chi}_z / \bar{\theta}_z, \overline{w'\chi'} + \overline{v'\theta'} \bar{\chi}_y / \bar{\theta}_z)$ is the eddy
 367 flux vector, and (v^*, w^*) are the meridional and vertical components of the residual cir-
 368 culation, respectively. Overbars denote zonal means and prime quantities indicate de-
 369 viations from it, while subscripts indicate partial derivatives. $H = 7$ km is the scale height,
 370 and $z \equiv -H \log_e(p/p_s)$ is the log-pressure altitude, with the surface pressure $p_s = 10^5$
 371 Pa. The S term is the net rate of change due to chemistry, defined as the difference be-
 372 tween the production (\bar{P}) and loss (\bar{L}) rates $\bar{S} = \bar{P} - \bar{L}$. The $\bar{\epsilon}$ contribution represents
 373 the residual of the budget, i.e., the difference between the actual rate of change of $\bar{\chi}$ and
 374 the sum of the transport and chemistry terms on the right-side hand of Eq. 1.

The transport terms in Eq. 1 can be grouped as follows:

$$\bar{\chi}_t = ADV + MIX + \bar{S} + \bar{\epsilon}, \quad (2)$$

375 where $ADV = (-v^* \bar{\chi}_y - w^* \bar{\chi}_z)$ and $MIX = e^{z/H} \nabla \cdot \mathbf{M}$ represent the contribution of
 376 the residual circulation and of the resolved mixing, respectively. We refer to M2020 for
 377 a more detailed description of the TEM framework applied to the N₂O mixing ratios in
 378 the stratosphere and for a comprehensive discussion of the contribution of each term to
 379 the N₂O budget.

380 2.6 Derivation of Trends with the Dynamical Linear Modelling Tool

381 In this study, we investigate decadal trends using the Dynamical Linear Modeling
 382 regression tool (DLM, Alsing, 2019). DLM is based on Bayesian inference and provides
 383 a number of possible models to analyze time series. Each model is characterized by some
 384 unknown parameters, and the DLM computes the posterior probability distribution of
 385 those parameters using a combination of Kalman filtering and Markov chain Monte Carlo
 386 method.

387 For a given atmospheric time-series y_t , a generic DLM model is composed of four
 388 components: a linear background trend, a seasonal cycle with 12- and 6-months periods,
 389 forcing terms described by a number of regressor variables and an auto-regressive com-

390 ponent:

$$\begin{aligned}
 391 \quad y_t &= \beta_{1,t}z_{1,t} + \beta_{2,t}z_{2,t} \dots + \beta_{n,t}z_{n,t} & (3) \\
 392 &+ \beta_{1,t}^{12} \sin(2\pi t/12) + \beta_{2,t}^{12} \cos(2\pi t/12) \\
 393 &+ \beta_{1,t}^6 \sin(2\pi t/6) + \beta_{2,t}^6 \cos(2\pi t/6) \\
 394 &+ \mu_t \\
 395 &+ z_t^{AR} \\
 396 &+ \epsilon_t.
 \end{aligned}$$

397 In Eq. 3, the terms $\beta_{i,t}z_{i,t}$ represent the contribution to y_t from the regressors, where
 398 $z_{i,t}$ is the corresponding time-series for each regressor. The 6- and 12-months seasonal
 399 cycles are modeled respectively by $\beta_{1,t}^6 \sin(2\pi t/6) + \beta_{2,t}^6 \cos(2\pi t/6)$ and $\beta_{1,t}^{12} \sin(2\pi t/12) +$
 400 $\beta_{2,t}^{12} \cos(2\pi t/12)$. The μ_t term denotes the linear fit term, and z_t^{AR} the auto-regressive
 401 term, defined similarly to the Cochrane-Orcutt correction (Kyrölä et al., 2013), and ϵ_t
 402 is the uncertainty.

403 Contrarily to a multi-linear regression (MLR) model, the background linear fit μ_t
 404 and the amplitudes of the seasonal cycles $\beta_{i,t}^{6,12}$ in DLM can vary with time (i.e., they
 405 are non-parametric). Their degrees of time-dependence are the unknown model param-
 406 eters and are initially set by the user and inferred from the data during the model run.
 407 Furthermore, the auto-regressive process in the DLM is computed within the model run
 408 together with the other parameters, not as a post-run correction as done in the MLR,
 409 and its uncertainties are carefully taken into account within the error propagation. In
 410 addition, the standard DLM implementation has time-varying (heteroscedastic) uncer-
 411 tainty distribution, when time-varying uncertainties are available. DLM was recently used
 412 to investigate stratospheric ozone trends in observations and models (Ball et al., 2017,
 413 2018). A more detailed description of the DLM models and their implementation can
 414 be found in Laine et al. (2014). For a more comprehensive review of time-series analy-
 415 sis using DLM, refer to Durbin and Koopman (2012).

416 As regressor variables, we used the 30 cm radio flux as a solar proxy (de Wit et al.,
 417 2014), an index for the El-Nino Southern Oscillation (Wolter & Timlin, 2011) from the
 418 National Oceanic and Atmospheric Administration (<http://www.esrl.noaa.gov/psd/enso/mei/>), and two indices for the QBO at 30 and 50 hPa from the Freie Universität
 419 Berlin (<http://www.geo.fu-berlin.de/en/met/ag/strat/produkte/qbo/index.html>).
 420 We fed the DLM model with monthly data, running 3000 samples where the first 1000
 421 were considered as a warmup and discarded. We also tried 10000 realizations and 3000
 422 as warmup with very similar results (not shown). We performed several sensitivity tests
 423 to determine the appropriate values of the initial model parameters, i.e., the degree of
 424 time-dependence of the linear trend and seasonal cycles, in order to allow a reasonable
 425 time-dependence without being unrealistic. The different combinations of these values
 426 did not provide significant differences, so we kept the recommended values.
 427

428 The linear trends are computed from the distribution of the fit samples μ_t as the
 429 difference between the end and start dates of the considered period ($\text{delta} = \mu_t[\text{end}] -$
 430 $\mu_t[\text{start}]$), weighted by the number of the years. From the resulting delta distribution,
 431 the uncertainties associated with the trend are computed as the percentage of its posi-
 432 tive (negative) values. This percentage can be interpreted as the posterior probability
 433 that the trend is positive (negative) between the considered dates. In this way, we do
 434 not make any assumption on the shape of the distribution of the trends.

435 3 Stratospheric N₂O Columns and their Trends

436 Figure 1 shows the linear fits of the monthly stratospheric N₂O columns (12-40 km)
 437 at the four FTIR stations, together with the initial N₂O columns from the observations

438 and the ERA5 simulation. In this analysis, we do not apply the FTIR time sampling to
 439 the model output because sensitivity tests using WACCM-REFD1 at each station showed
 440 no significant impact of the FTIR time sampling on the recovered trends of the N₂O columns
 441 (not shown). The stratospheric N₂O columns computed between 12 and 40 km of alti-
 442 tude are highly sensitive to the N₂O increase in the lower stratosphere, which is mainly
 443 the result of the continuous growth in the troposphere (Tian et al., 2020) and can also
 444 be impacted by structural changes of the atmosphere (e.g., the global rise of the tropopause,
 445 Xian & Homeyer, 2019). Consequently, all datasets exhibit an increase in the stratospheric
 446 N₂O columns over the last two decades.

447 Above Lauder, the linear fit of the stratospheric N₂O columns from the ERA5 sim-
 448 ulation is in agreement with the observations, similarly to JRA55 and ERAI. WACCM-
 449 REFD1 underestimates the stratospheric N₂O columns compared to the observations by
 450 around 10%, and performs worse than its earlier version WACCM-REFC1, which dif-
 451 fers from the observations by only 5%. At Wollongong, the slope of the linear fit of the
 452 N₂O columns measured by the FTIR, and to a lesser extent by ACE-FTS, is steeper be-
 453 fore 2005 compared to the following period. This change of gradient is not visible in any
 454 of the model simulations. On the contrary, some of the models show a slower increase
 455 before 2005, followed by a more rapid increase (e.g., the ERA5 simulation). Contrarily
 456 to Lauder, the WACCM-REFD1 simulation delivers more realistic stratospheric N₂O columns
 457 compared to its previous version WACCM-REFC1.

458 Above Izaña, all the models underestimate the stratospheric N₂O columns with re-
 459 spect to the FTIR observations, with the largest difference reaching 14% for MERRA2.
 460 Concerning ACE-FTS, the bias with FTIR measurements is around 8%, which is qual-
 461 itatively consistent with the results of Strong et al. (2008), even though they used v2.2
 462 of ACE-FTS. However, García et al. (2021) showed good agreement above Izaña for tropo-
 463 spheric N₂O abundances and total N₂O columns obtained from independent measure-
 464 ments. The difference between the stratospheric N₂O columns measured by FTIR and
 465 ACE-FTS could be explained by the poor coverage of ACE-FTS over the tropical and
 466 subtropical regions. Since the ACE-FTS measurements represent a latitude band, the
 467 observed N₂O results biased towards the values measured at higher latitudes, where more
 468 occultations are available (Kolonjari et al., 2018). Since the N₂O abundances decrease
 469 poleward (Jin et al., 2009), this could explain the low bias in the stratospheric N₂O columns
 470 measured by ACE-FTS compared to those obtained from FTIR.

471 Above Jungfraujoch, there is the largest spread in the linear fits of the stratospheric
 472 N₂O columns, with the largest differences reaching around 25% between ACE-FTS and
 473 WACCM-REFD1. Prignon et al. (2019) compared lower stratospheric columns of chlorod-
 474 ifluoromethane (HCFC-22) between an earlier WACCM version and FTIR measurements,
 475 and showed that WACCM consistently underestimates the HCFC-22 columns compared
 476 to the FTIR measurements. Since both N₂O and HCFC-22 (which has an atmospheric
 477 lifetime of 12 years, Prignon et al., 2019) are produced at the surface and transported
 478 into the stratosphere, this underestimation in WACCM could indicate a shortcoming in
 479 simulating the accumulation of long-lived tracers in the stratosphere above the north-
 480 ern mid-latitudes. Indeed, Angelbratt et al. (2011) already highlighted that the strato-
 481 spheric transport has a large impact on the N₂O columns above Jungfraujoch compared
 482 to stations at higher latitudes. Regarding the observational datasets, there is a consid-
 483 erable disagreement between the FTIR instrument and ACE-FTS before 2012, showing
 484 increasing and decreasing N₂O columns, respectively. This is in contrast with the remark-
 485 ably good agreement in the SH between the two datasets. This difference between the
 486 stratospheric N₂O columns in ACE-FTS and FTIR measurements will be further addressed
 487 in Sect. 4.

488 In the Tropics and above the lower stratospheric mid-latitudes, the N₂O abundances
 489 are inversely proportional to the mean AoA (Andrews et al., 2001; Strahan et al., 2011;
 490 Galytska et al., 2019). The stratospheric N₂O columns at mid-latitudes considered here

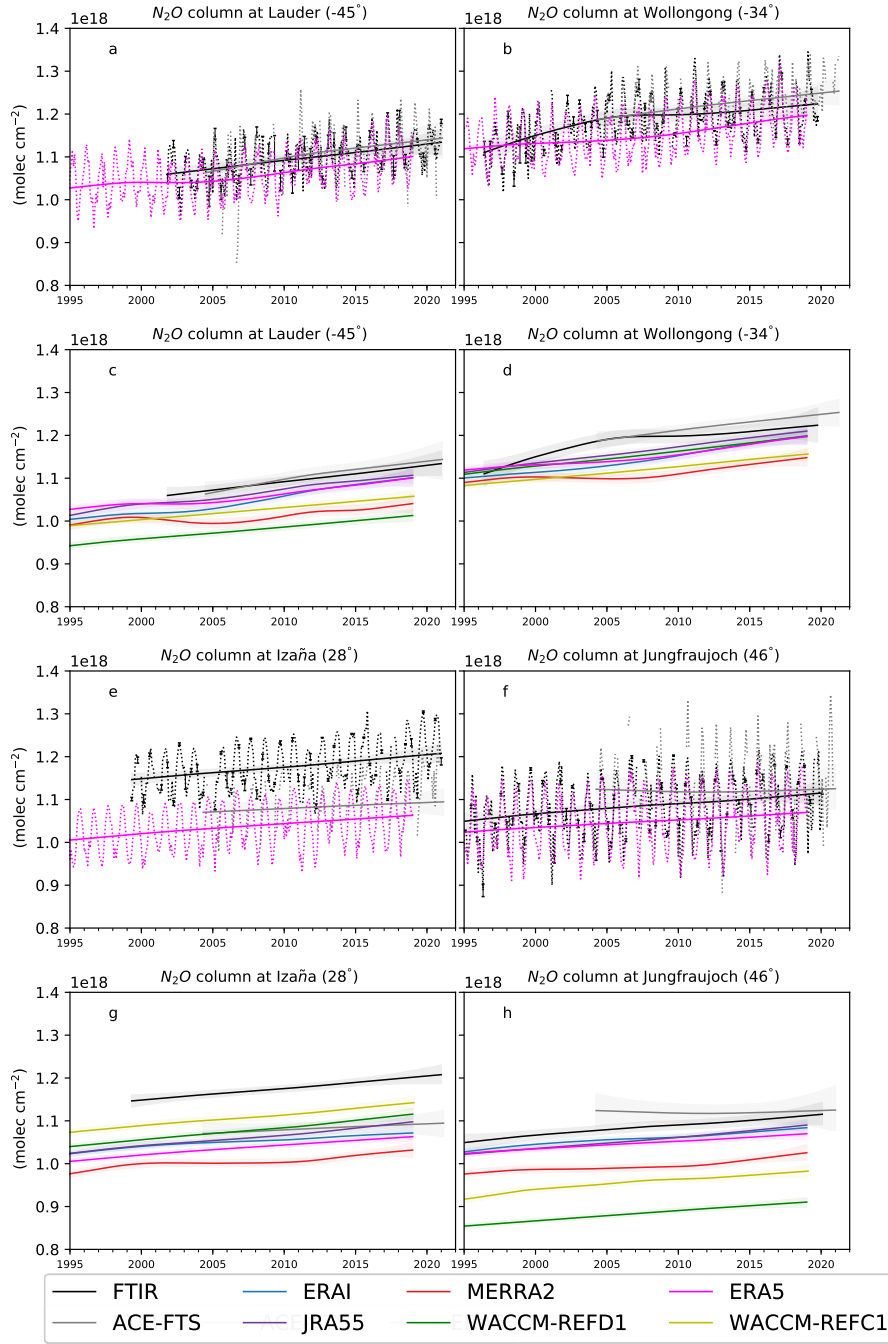


Figure 1. Time-series of stratospheric N_2O columns (12-40 km) from observations and models at four stations. Continuous lines show the linear fit obtained by the DLM regression, dashed lines depict the N_2O column data. The color code is shown in the legend. The vertical error bars in panels a,b,e,f represent the standard error of the monthly mean. Panels a,b show Lauder, panels b,d show Wollongong, panels e,g show Izaña and panels f,h show Jungfraujoch. Panels a,b,e,f: DLM fits and data for FTIR and ACE-FTS measurements and the BASCOE simulation driven by ERA5. Panels c,d,g,h: DLM fits for all the datasets considered. The model and satellite data are interpolated to the longitude and latitude of the station, and vertically regridded to match the retrieval layering schemes. After the regridding, the data were smoothed using the FTIR averaging kernels. The colored shadings represent the uncertainties from the 2.5 and 97.5 percentiles of the distributions from the DLM.

491 are highly sensitive to the N₂O abundances in the lower stratosphere, hence the inverse
 492 relationship also holds for the stratospheric N₂O columns above the mid-latitudes. Thus,
 493 the lower stratospheric N₂O columns in MERRA2 compared to the other datasets across
 494 the stations are consistent with the older mean AoA throughout the stratosphere found
 495 using MERRA2 by Chabrillat et al. (2018). The N₂O distribution in the stratosphere
 496 is opposite also to the total inorganic fluorine F_y. N₂O is emitted in the troposphere while
 497 F_y is produced in the stratosphere, and, as a consequence of the poleward transport of
 498 the BDC, N₂O is removed and F_y is increased in the stratospheric mid-latitudes. In the
 499 light of this relationship between N₂O and F_y, the underestimated N₂O columns above
 500 Lauder and Jungfraujoch in MERRA2 are consistent with larger stratospheric F_y columns
 501 in MERRA2 compared to the other reanalyses above those stations (Prignon et al., 2021).

502 Figure 2 shows distributions of the trend of the stratospheric N₂O columns obtained
 503 from the respective linear fits over the common period 2005-2018. The N₂O trends at
 504 the surface have already been compared for a number of FTIR stations (including Lauder,
 505 Wollongong and Izaña) against observations from flask samples, showing an excellent agree-
 506 ment (Zhou et al., 2019).

507 Above Lauder, the N₂O trends obtained with ERA5 and JRA55 are in good agree-
 508 ment with the FTIR measurements, but are underestimated in WACCM-REFD1 (around
 509 25%) with no particular improvement with respect to WACCM-REFC1. The ERAI sim-
 510 ulation delivers the largest N₂O trends, with more than 30% difference with respect to
 511 the FTIR measurements. At Wollongong, the N₂O trend obtained with the FTIR mea-
 512 surements is the smallest because the N₂O increase above that station is smoother com-
 513 pared to the other datasets. Interestingly, the N₂O trend simulated by WACCM-REFD1
 514 is the closest to the trend obtained from the FTIR observations, while the trend obtained
 515 with ERA5 is almost twice as large. As for Lauder, the N₂O trends obtained from ERAI
 516 are the largest at this station. Above Izaña, WACCM-REFD1 agrees remarkably well
 517 with the FTIR (difference around 3%), while the trend from ERA5 lies between the trends
 518 measured from FTIR and ACE-FTS, with around 20% difference compared to FTIR.
 519 Above Jungfraujoch, the trend in the N₂O columns from WACCM-REFD1 agrees with
 520 the trend from the FTIR within 10% difference and is similar to what is obtained with
 521 ERA5. The largest trends are obtained with MERRA2 and JRA55, reaching 13% and
 522 30% difference compared to the FTIR, respectively. The decreasing N₂O stratospheric
 523 column in ACE-FTS before 2012 results in a near-zero trend, which is in contrast with
 524 the trends obtained by the other datasets, which approximately range from 2 to 3 × 10¹⁵
 525 molec cm⁻² year⁻¹.

526 Considering decadal changes, the observations and the ERA5 and ERAI simula-
 527 tions show larger trends of the stratospheric N₂O columns in the SH than in the NH,
 528 especially at mid-latitudes (respectively Lauder and Jungfraujoch). WACCM-REFD1
 529 also shows this hemispheric difference at mid-latitudes, which is a clear improvement with
 530 respect to WACCM-REFC1. Those asymmetries are consistent with the results of Strahan
 531 et al. (2020), who found significantly negative mean AoA trends in the SH compared to
 532 the NH using HCl and HNO₃ measured at several ground-based FTIR stations. In ad-
 533 dition, the hemispheric differences of the N₂O trends are also consistent with the results
 534 of Prignon et al. (2021), who found larger and more significant F_y trends from FTIR above
 535 Jungfraujoch than above Lauder.

536 We conclude the section by providing a short description of the limits of using strato-
 537 spheric columns of N₂O from FTIR measurements. As mentioned earlier, the stratospheric
 538 N₂O columns between 12 and 40 km are primarily influenced by the steady increase in
 539 the lowermost stratosphere below 15 km. The DOFS of the FTIR instrument at Jungfrau-
 540 joch for the stratosphere (12-40 km) is close to 1.1. Thus, the FTIR measurements at
 541 that station cannot resolve more than one partial column between 12 and 40 km, which
 542 can hinder the detection of N₂O trends in the middle and upper stratosphere (i.e., above
 543 30 km) because of the influence of the increase in the lowermost stratosphere. Indeed,

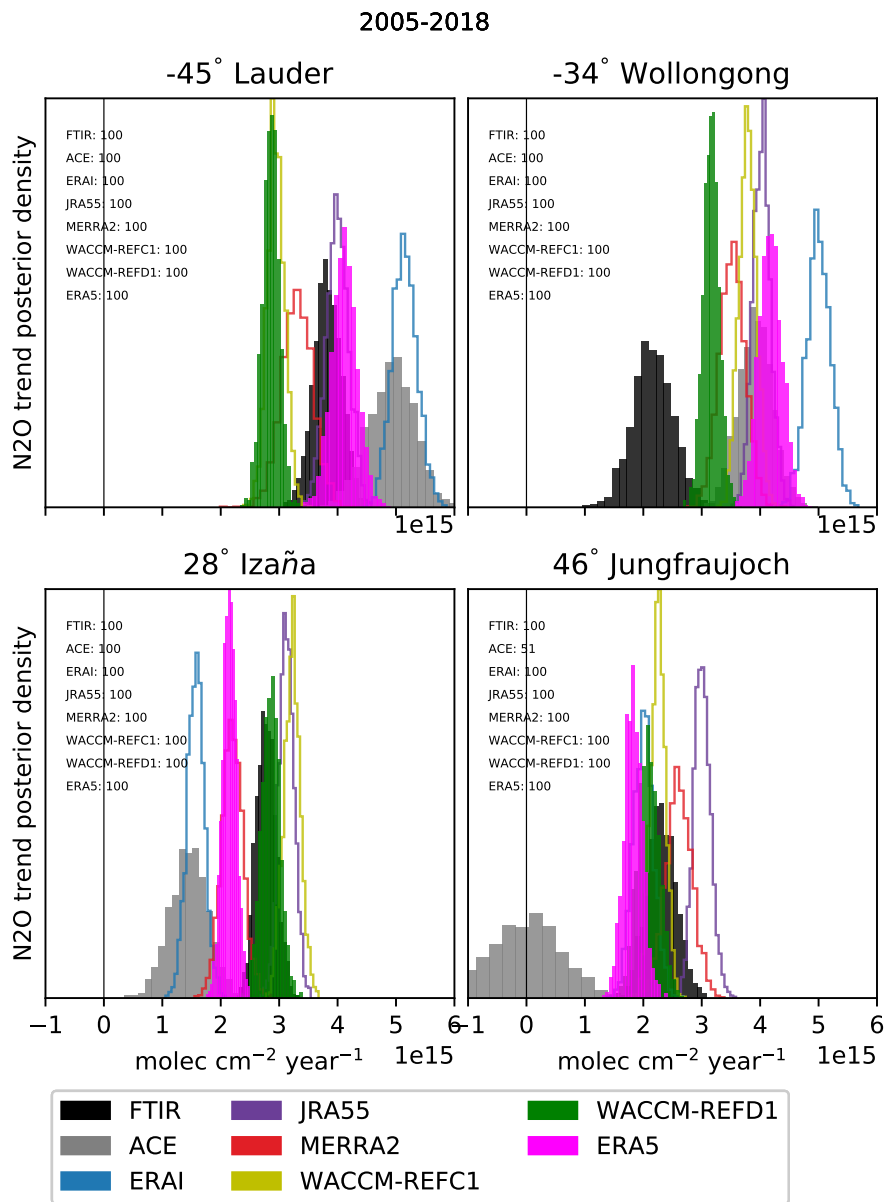


Figure 2. Posterior probability of positive changes of the DLM linear trend of the stratospheric N₂O columns (12-40 km) for the four FTIR stations (2005-2018). The color code is shown in the legend. For reference, the N₂O trend in the troposphere (5.5-10.5 km) is approximated from the data in Bernath et al. (2020) as 4.3e15 molec cm⁻² year⁻¹.

544 it was shown that stratospheric N₂O trends over the last decades, obtained both from
 545 satellite measurements and model simulations, do not consist of just a global increase,
 546 but largely depend on latitude and height (e.g., Froidevaux et al., 2019). Therefore, we
 547 will consider latitudinal- and vertical-dependent trends of N₂O mixing ratios in the fol-
 548 lowing section.

549 4 Global N₂O Linear Trends

550 4.1 Trends in the ACE-FTS Observational Space

551 Figure 3 shows latitude-vertical cross sections of the linear trends of the N₂O mix-
 552 ing ratios for the various datasets, over the 2005-2018 period. In order to reduce the sam-
 553 pling bias, the model datasets are sampled in space and time as the ACE-FTS measure-
 554 ments before the computation of the trends. We use the ACE-FTS measurements as a
 555 reference, because they encompass this period with global coverage and good stability
 556 (Bernath et al., 2020, 2021).

557 In the upper stratosphere above 10 hPa, the N₂O trends from ACE-FTS are pos-
 558 itive, with larger trends in the NH that are found significant at lower levels than in the
 559 SH. The ERAI-driven simulation qualitatively reproduces these patterns in the upper
 560 stratosphere, while the other model datasets differ from ACE-FTS, especially ERA5. A
 561 common feature among all datasets is an increase in N₂O above the Equator in the up-
 562 per stratosphere, around 5 hPa. At those altitudes of the tropical pipe, the upward trans-
 563 port of N₂O by the residual circulation reaches its maximum (see M2020).

564 In the mid-lower stratosphere below 20 hPa, ACE-FTS shows a clear hemispheri-
 565 cal asymmetry (meridional dipole) in the N₂O trends, with significantly negative val-
 566 ues in the NH and significantly positive in the SH. Above the location of Jungfrau-
 567 joch (the most northern vertical green line), the negative N₂O trend detected by ACE-FTS
 568 in the mid-lower stratosphere is responsible for the disagreement with the FTIR obser-
 569 vations discussed in the previous section, as the layer of the stratospheric N₂O column
 570 encompasses regions of both positive (lowermost and upper stratosphere) and negative
 571 (mid-lower stratosphere) N₂O trends. The meridional dipole is significant also over a shorter
 572 period (2005-2012, not shown) and corroborates a number of previous findings over that
 573 period using satellite measurements of HCl (Mahieu et al., 2014) and mean AoA derived
 574 from space-borne measurements of SF₆ (Haenel et al., 2015). In regions where the N₂O
 575 abundances are larger than 100 ppbv, i.e., approximately below 10 hPa, the N₂O linear
 576 trends are opposite to those obtained with its product NO₂, because the two tracers are
 577 correlated by an inverse linear relationship (Plumb & Ko, 1992). Below 20 hPa, the N₂O
 578 meridional dipole from ACE-FTS is consistent with the pattern of the decadal trends
 579 of NO₂ obtained from independent satellite measurements (Galytska et al., 2019; Dubé
 580 et al., 2020).

581 The meridional dipole in the N₂O trends derived from ACE-FTS is generally re-
 582 produced by the CTM simulations, with ERAI and ERA5 delivering trends that are most
 583 similar to the satellite measurements. Prignon et al. (2021) used the same simulations
 584 as the present study to investigate global stratospheric trends of total inorganic fluorine
 585 F_y. The dipoles obtained here in the N₂O trends from the ECMWF reanalyses are con-
 586 sistent with the opposite trends of F_y for almost the same period (Prignon et al., 2021).
 587 For WACCM, the strength of the N₂O meridional dipole is globally reduced compared
 588 to ACE-FTS, with weaker and not significant negative N₂O trends over the NH. How-
 589 ever, WACCM-REFD1 performs better than WACCM-REFC1 over the SH, with stronger
 590 and significant positive N₂O trends that reach 30 hPa, similarly to those obtained with
 591 ACE-FTS in the same region. This improvement is possibly related to the changes in
 592 the parametrization of the gravity waves (i.e., small-scale tropospheric waves that drive
 593 the BDC) in WACCM version 6 compared to version 4 that followed the increase of its

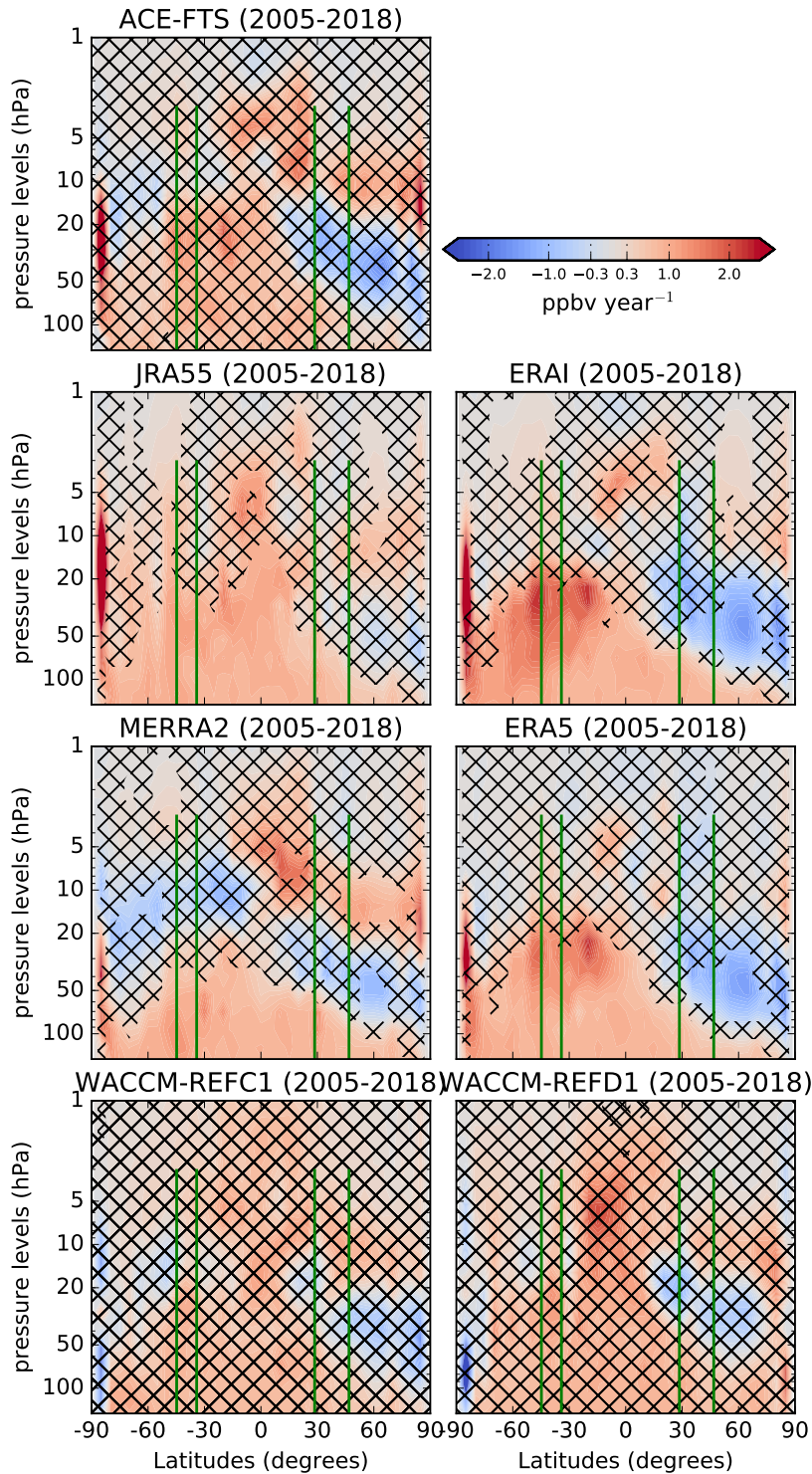


Figure 3. Latitude-pressure cross-sections of N_2O linear trends (pptv year^{-1}) obtained from the DLM (2005-2018). The N_2O simulated by the model is interpolated to the location and timing of the observations, see text for details. The black crosses indicate grid-points where the probability of positive/negative N_2O changes is smaller than 95%. The green vertical lines identify the position of the FTIR stations together with their vertical coverage.

horizontal resolution (Gettelman et al., 2019). This new parametrization results in a good agreement between the gravity waves simulated by WACCM and the observations in the Tropics (Alexander et al., 2021). For tracers, the favorable effect of adjusting the parameterization of the gravity waves in WACCM was shown for ozone in the extratropical SH by Mills et al. (2017). Over the same region, the improved N₂O trends in WACCM-REFD1 compared to WACCM-REFC1 could be attributed to the new parameterization of the gravity waves. This beneficial impact would be consistent with the results of M2020, which showed similar improvements in the N₂O climatologies between two WACCM versions differing by the parametrization of gravity waves over the SH.

In the lowermost stratosphere (pressure greater than 100 hPa), all models and ACE-FTS show positive N₂O trends, resulting from the constant increase in the troposphere. However, the N₂O increase in the lowermost stratosphere (below 70 hPa) over the Tropics and the NH is not significant in ACE-FTS, contrary to the model simulations. This difference could be related to the stronger trends in the tropopause rise in the models: around 50 m/decade in CCMs (including WACCM) and ERA5 (Pissoft et al., 2021; Darrag et al., 2022) compared to the observations (around 35 m/decade, Darrag et al., 2022) when using the tropopause definition from the World Meteorological Organization.

4.2 Trends in the Model Space

Figure 4 shows the N₂O trends as in Fig. 3, but without applying the ACE-FTS spatial and temporal sampling. A comparison between each model simulation in the observation and model space (respectively Fig. 3 and Fig. 4) reveals large differences in the N₂O decadal trends. Generally, the sampling of the ACE-FTS observations enhances the trends simulated by the models, both in the negative and positive directions. For the ERA5 simulation, the significantly negative trend in the NH in observational space becomes insignificant in model space. In addition, one notes immediately that the N₂O trends in the WACCM simulations change sign, with negative trends in the NH in the observational space becoming weakly positive in model space. In particular for WACCM-REFD1, the N₂O trends over the northern mid-latitudes in the mid-low stratosphere substantially increase from -0.5 ppbv year⁻¹ in observational space to 0.3 ppbv year⁻¹ in native model space. However, this difference is not significant because neither of the N₂O trends above that region is statistically significant with 95% probability.

For satellite measurements, the impact of the sampling in the detection of trends in long-lived species (including N₂O) has been evaluated in Millán et al. (2016). They concluded that large errors may arise in the detected trends for coarse and non-uniform sampling obtained with occultation instruments (such as ACE-FTS), and that long time scales are required for a robust trend detection from these datasets. Such errors also occur in the models when they are sampled in space and time as the observations. In particular, within the DLM, the non-uniform time sampling of ACE-FTS considerably increases the standard deviation of the error in the N₂O time series, which is zero for regular time sampling. This difference plays a role when deriving trends over these relatively short (decadal) time scales. For example, the non-uniform ACE-FTS sampling applied to the ERA5 output results in negative N₂O trends that are 4 times stronger compared to the native grid above the northern mid-latitudes between 50 and 70 hPa. For WACCM, the issue of downsampling was also raised by Garcia et al. (2011) when comparing mean AoA trends obtained from balloon-borne observations and simulated by the model. Garcia et al. (2011) showed that sampling the model as the observations would deliver positive and non-significant mean AoA trends, similarly to the observations. We find consistent results with the WACCM simulations: sampling the WACCM output as the observations drives the N₂O trends towards the observed values. In addition, the non-significant negative N₂O trends simulated by WACCM are compatible with the non-significant positive mean AoA trends found by Garcia et al. (2011) when downsampling WACCM at

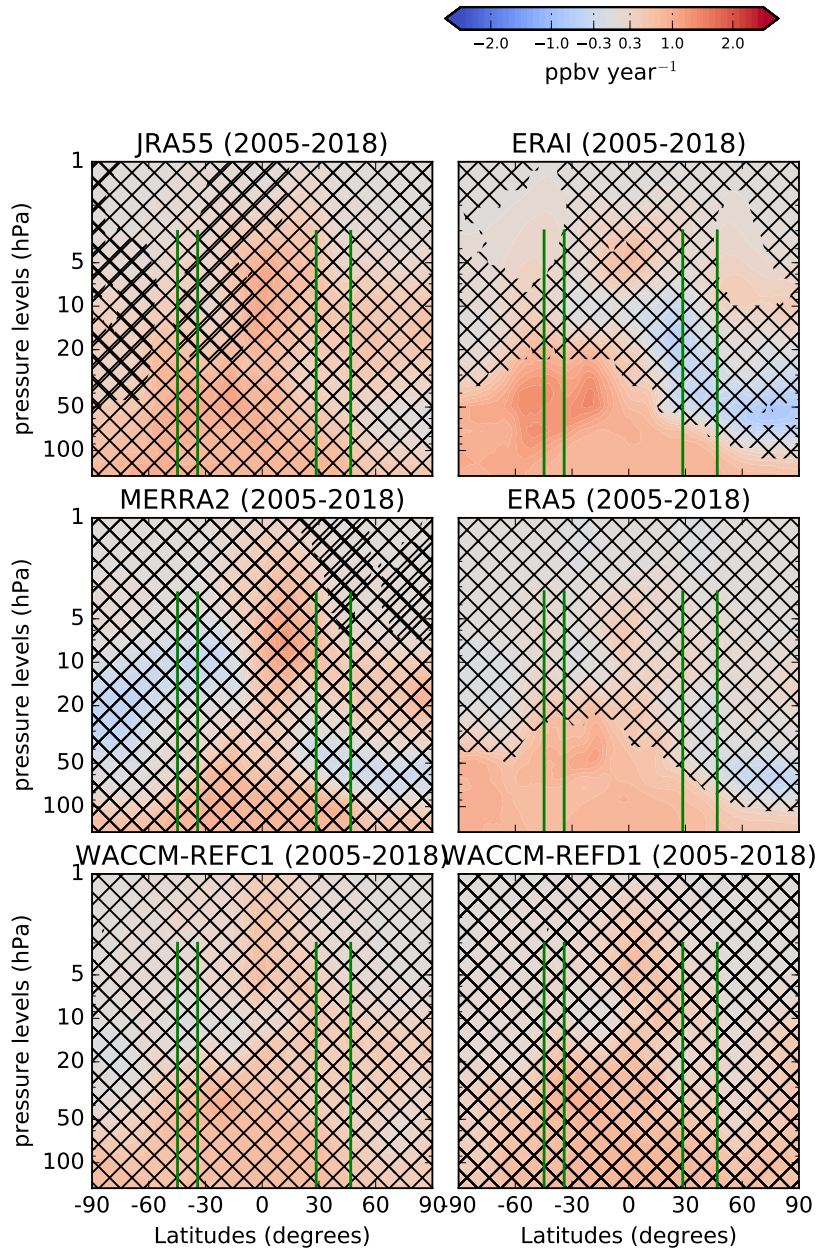


Figure 4. As in Figure 3, but in the model space.

645 the mean AoA observations. Hence, the ACE-FTS sampling exaggerates the simulated
 646 N₂O trends obtained with the DLM in the stratosphere.

647 In order to understand the trends from the models and compare them with other
 648 modeling studies, we now focus on the N₂O trends obtained from the model datasets in
 649 model space (Fig. 4). We mentioned earlier that the mean AoA and the N₂O abundances
 650 are inversely correlated in the Tropics and above the lower stratospheric mid-latitudes.
 651 Thus, the stratospheric N₂O trends have opposite signs compared to trends of mean AoA.
 652 For ERAI, the meridional N₂O trend dipole is consistent with mean AoA trends derived
 653 over a shorter period with the same CTM (Chabrilat et al., 2018) and also with differ-
 654 ent CTMs (Ploeger et al., 2015; Han et al., 2019; Ploeger & Garny, 2022). ERAI shows
 655 positive N₂O trends in the equatorial upper stratosphere, around 5 hPa, which is con-
 656 sistent with the findings of Galytska et al. (2019) using the same reanalysis to drive a
 657 different CTM in that region, but no significant trend can be found with ERA5 in the
 658 upper stratosphere. The ERA5 simulation confirms the meridional dipole in the mid-
 659 lower stratosphere of ERAI, although the negative N₂O trend over the NH is not sta-
 660 tistically significant at 95% probability. The results obtained with ERA5 are consistent
 661 with recent N₂O and mean AoA trends obtained with a different CTM over a very sim-
 662 ilar period (Ploeger & Garny, 2022).

663 Above the southern mid-latitudes in the mid-lower stratosphere, the N₂O trends
 664 obtained with MERRA2 are biased low compared to the other models, and do not repli-
 665 cate the hemispheric asymmetry that is visible in the ECMWF reanalyses. Wargan et
 666 al. (2018) have shown that the tropopause height has changed in MERRA2 in the past
 667 decades, with a decrease in the extratropics and an increase above the Tropics. The pat-
 668 tern of the N₂O trends in MERRA2 is qualitatively consistent with the changing tropopause
 669 height: a rise of the tropopause would lead to positive N₂O trends, while a sinking tropopause
 670 would lead to negative N₂O trends. In addition, the patterns of the N₂O trends obtained
 671 with MERRA2 disagree with those obtained with the same reanalysis using a different
 672 CTM (Ploeger & Garny, 2022), and do not match the mean AoA trends obtained with
 673 the same CTM (Chabrilat et al., 2018), at least in the regions where the inverse rela-
 674 tionship between N₂O and mean AoA holds (Galytska et al., 2019). The large differences
 675 between JRA55 and MERRA2 and the ECMWF reanalyses in the extratropical mid-
 676 stratosphere highlight that decadal changes in the stratospheric transport are not as ro-
 677 bustly detected in JRA55 and MERRA2 as in the ERAI and ERA5. In the equatorial
 678 lower stratosphere, all the CTM simulations deliver a significant N₂O increase, which
 679 can partly be attributed to the effect of the tropopause rise that was robustly detected
 680 in the reanalyses in the past decades (Manney & Hegglin, 2018).

681 WACCM does not simulate the N₂O decrease in the northern polar stratosphere
 682 seen in the ECMWF reanalyses, but rather a global N₂O increase that is largest in the
 683 lower stratosphere. The N₂O increase in the tropical lower stratosphere can be related
 684 to the structural changes of the stratosphere in response to global warming that were
 685 robustly predicted in CCMs (e.g., Oberländer-Hayn et al., 2016; Šácha et al., 2019; Eichinger
 686 & Šácha, 2020). As discussed in the previous Section, WACCM-REFD1 improves the
 687 representation of the N₂O trends with respect to WACCM-REFC1 in the southern mid-
 688 latitudes. The newer WACCM version simulates a significant N₂O increase up to 20 hPa,
 689 which makes the N₂O trends in the southern mid-lower stratosphere more similar to those
 690 from ERAI and ERA5, even though the decreasing N₂O trends in the NH are not re-
 691 produced. As discussed in the previous Section, this improvement in the N₂O trends over
 692 the SH could be attributed to the adjusted parametrization of gravity waves in version
 693 6 of WACCM compared to its version 4.

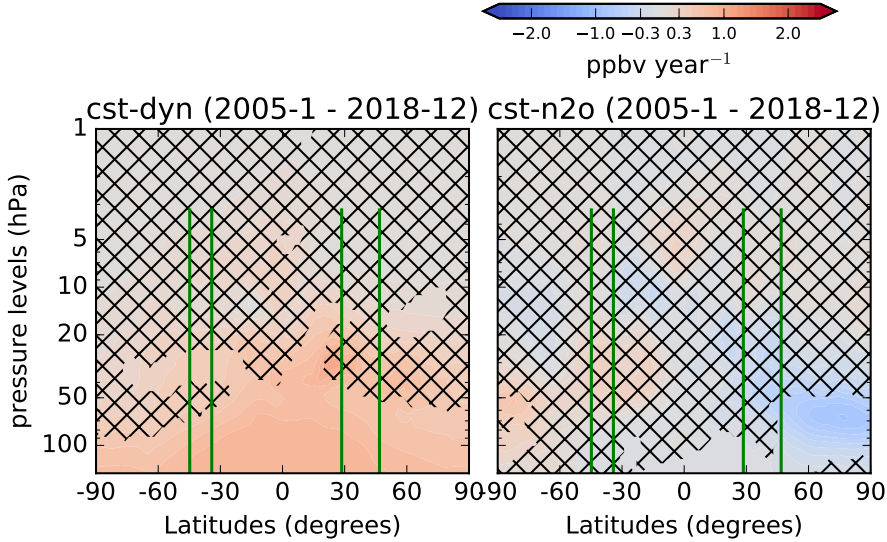


Figure 5. Latitude-pressure cross sections of N_2O linear trends (pptv year^{-1}) obtained from the DLM from a BASCOE run driven by ERA5 with fixed dynamics and increasing N_2O (left panel), and from the same model setup but with N_2O kept constant at the surface and time-varying dynamics (right panel). The black crosses indicate grid-points where the probability of positive/negative N_2O changes is smaller than 95%. The green vertical lines identify the position of the FTIR stations together with their vertical coverage.

694 Figure 5 shows the N_2O trends obtained from the two sensitivity tests done with
 695 ERA5 (cst-dyn and cst- N_2O). As expected, the cst-dyn experiment does not simulate
 696 any N_2O decrease in the stratosphere, showing only a steady N_2O increase as a conse-
 697 quence of the constant buildup at the surface. Between 30 and 50 hPa, the N_2O increase
 698 in the SH is significant with 95% probability, while this is not the case over the NH. This
 699 difference can be attributed to the larger variability of the NH over one QBO cycle com-
 700 pared to the SH due to its larger wave activity (Scaife & James, 2000), and was already
 701 shown for the significance of ozone trends (Shepherd, 2008). This highlights the impor-
 702 tance of considering a sufficiently long period for the trend detection in the stratosphere
 703 (Garcia et al., 2011; Hardiman et al., 2017; Strahan et al., 2020). In particular, the 14
 704 years considered here are sufficient to propagate the N_2O increase to the mid-stratospheric
 705 mid-latitudes in the SH but not in the NH. The cst- N_2O sensitivity test confirms that
 706 the extratropical N_2O trends in the mid-lower stratosphere are due to the impact of changes
 707 in the stratospheric transport. In addition, Ploeger and Garny (2022) recently showed
 708 that structural changes of the stratospheric circulation also determine the hemispheric
 709 asymmetry in the N_2O trends in the reanalyses. Contrarily to the cst-dyn experiment,
 710 a changing dynamics impacts the sign of the obtained trends, with an N_2O decrease above
 711 the NH and increase in the SH. From these sensitivity tests, we show that both the mean
 712 stratospheric transport and its decadal changes can contribute to the hemispheric asym-
 713 metry in the recovered N_2O trends. The mean stratospheric transport contributes with
 714 differences in the significance of the N_2O trends, and the decadal changes in the strato-
 715 spheric transport with differences in their respective signs.

716 5 N_2O TEM Budget

717 This section further investigates the N_2O trends from the model simulations using
 718 the TEM budget. Equation 2 allows separating the contributions of the residual cir-

719 culation and mixing terms (respectively *ADV* and *MIX*) to the N₂O rate of change. In
 720 particular, we aim to identify the contributions from changes in the *ADV* and *MIX* terms
 721 to the N₂O trends shown in the previous section (Fig. 4). To that end, we compute the
 722 changes of the *ADV* and *MIX* terms as the differences between their linear fits (i.e., the
 723 μ_t term of Eq. 3) at the end and the beginning of the considered period. A similar anal-
 724 ysis was also done in the recent study of Abalos et al. (2020), who used the outputs of
 725 several CCMs to compute changes of the TEM budget terms of synthetic tracers. For
 726 a detailed description of the climatologies of the *ADV* and *MIX* terms, we refer to M2020.

727 Here, we provide a qualitative analysis of the contributions from changes in the ad-
 728 vection and mixing to the N₂O trends, by comparing the signs of the changes of *ADV*
 729 and *MIX* with those of the N₂O trends discussed in the previous section. With this ap-
 730 proach, we aim to evaluate separately the contributions from changes in *ADV* and *MIX*
 731 to the N₂O trends, and we do not consider their compensation mechanisms that arise
 732 from the common driving from the breaking of tropospheric waves (M2020). The com-
 733 plete N₂O TEM budget also includes the chemistry term \bar{S} (i.e., loss due to photolysis,
 734 Tian et al., 2020), which is large in the tropical mid-high stratosphere, and the residual
 735 term $\bar{\epsilon}$, which accounts for all the processes not resolved by the TEM analysis (includ-
 736 ing mixing on unresolved scales, Eq. 2). Figure 6 shows the latitude-vertical cross sec-
 737 tions of those changes in the *ADV* and *MIX* terms over 2005-2018. We limit the anal-
 738 ysis to the simulations by ERA5 and WACCM-REFD1 in order to investigate further
 739 the differences in their N₂O trends discussed in the previous section. In the following,
 740 we refer to N₂O trends discussed in the previous section as "direct" N₂O trends, in or-
 741 der to distinguish them from the N₂O changes derived from changes in the *ADV* and
 742 *MIX* contributions.

743 Considering the changes in the *ADV* term, the ERA5 and WACCM-REFD1 sim-
 744 ulations agree over the tropical high stratosphere (above 5 hPa), with a significant in-
 745 crease of the N₂O abundances due to the impact of the residual circulation, similar to
 746 the weak positive direct N₂O trends in the same region in both simulations. Over this
 747 region, the main contribution to the *ADV* term is the transport due to the vertical com-
 748 ponent of the residual circulation, i.e., $-w^*\bar{\chi}_z$ in Eq. 1 (M2020). We found that the *ADV*
 749 changes are mainly due to an enhanced tropical upwelling $-w^*$ over the tropical high
 750 stratosphere rather than to changes of the N₂O vertical gradients $\bar{\chi}_z$ (not shown). These
 751 results of *ADV* changes agree with recent studies showing a strengthening of the advec-
 752 tive part of the BDC over the Tropics over longer periods in ERA5 (Diallo et al., 2021)
 753 and in version 6 of WACCM (Abalos et al., 2021). In the northern subtropics in the lower
 754 stratosphere, both WACCM-REFD1 and the CTM driven by ERA5 consistently sim-
 755 ulate positive N₂O changes due to an enhanced *ADV* contribution that can contribute
 756 to the positive direct N₂O trend over the same region. This significant contribution from
 757 *ADV* can be associated with the strengthening of the shallow branch of the BDC (Lin
 758 & Fu, 2013), which was recently detected in ERA5 using the AoA diagnostic (Ploeger
 759 et al., 2021) and predicted by CCMs (Butchart, 2014). In the mid-latitudes in both hemi-
 760 spheres, the changes in the *ADV* term are largely non-significant in both datasets, es-
 761 pecially in WACCM-REFD1, and do not correspond to any direct N₂O trend, prevent-
 762 ing to draw robust conclusions. In the polar regions, WACCM-REFD1 and the CTM
 763 driven by ERA5 disagree over the Antarctic, where the CCM simulates negative *ADV*
 764 changes, while the CTM shows positive non-significant changes across almost the whole
 765 stratosphere. In the Arctic, the two simulations agree well in the lower stratosphere (be-
 766 low 30 hPa) with negative changes of the *ADV* term that can explain the negative di-
 767 rect N₂O trend and are consistent with the enhanced *ADV* term over the tropical re-
 768 gion.

769 Concerning the *MIX* term, its changes are more irregular compared to those of
 770 the *ADV* term in both WACCM-REFD1 and ERA5, and do not correspond to the di-
 771 rect N₂O trends over the NH. In addition, the *MIX* changes obtained with the CCM

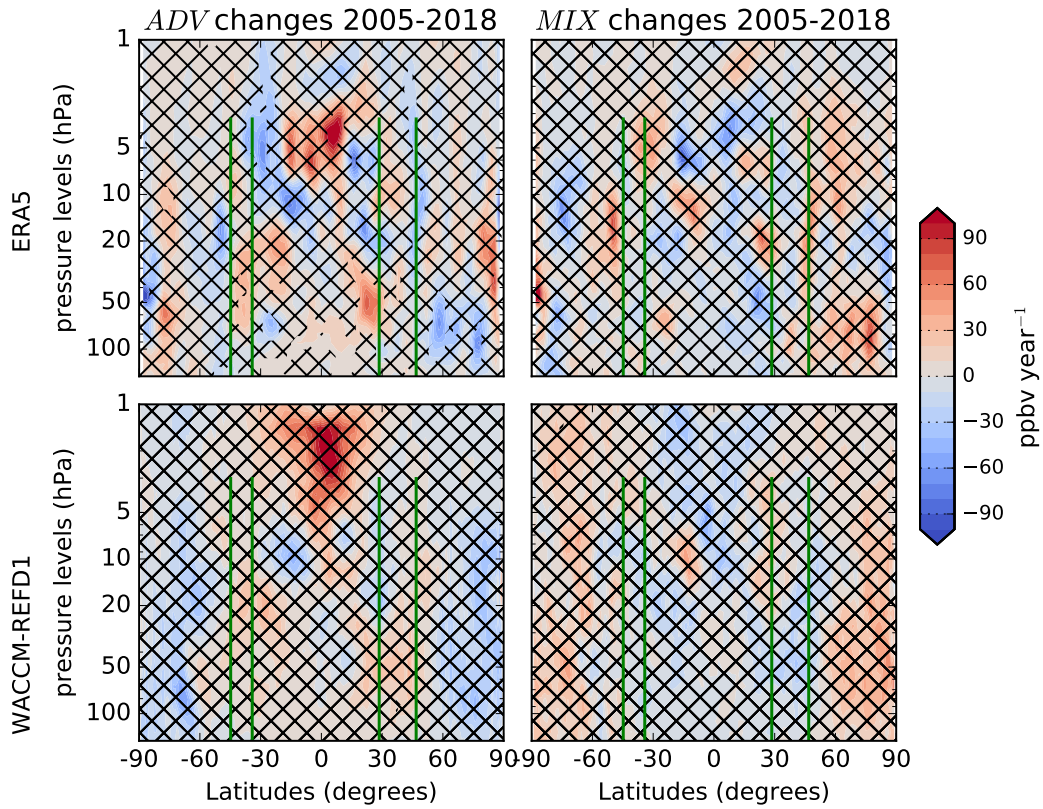


Figure 6. Latitude-pressure cross sections of the changes of the advection term ($A_z + A_y$, left panels, ppbv year⁻¹) and mixing term ($M_z + M_y$, right panels, ppbv year⁻¹) of the TEM N₂O budget for ERA5 (top) and WACCM-REFD1 (bottom) for 2005-2018. The black crosses indicate grid-points where the probability of positive/negative N₂O changes is smaller than 95%. The green vertical lines identify the position of the FTIR stations together with their vertical coverage.

772 largely disagree with those from the CTM and their significance is considerably smaller.
 773 Large differences between WACCM and the CTM driven by reanalyses were already shown
 774 by M2020 for the climatologies of the mixing terms of the N₂O TEM budget. Further-
 775 more, the weaker effect of mixing in WACCM-REFD1 compared to ERA5 is consistent
 776 with Dietmüller et al. (2017), who found weaker AoA trends in the resolved aging by mix-
 777 ing in a free-running CCM compared to its specified-dynamics version and a reanalysis.
 778 Concerning the *MIX* term in ERA5, in the SH between 10 and 30 hPa, there is enhanced
 779 poleward mixing that transports N₂O from the subtropics (where *MIX* changes are neg-
 780 ative) to the mid-latitudes (where the *MIX* changes are positive). Such positive N₂O
 781 changes in the southern mid-latitudes can be associated with the positive but not sig-
 782 nificant direct N₂O trends over the same region. The role of both resolved and unresolved
 783 mixing in the decadal BDC trends has been studied in ECMWF reanalyses, especially
 784 using AoA (e.g., Ploeger et al., 2015; Dietmüller et al., 2017). Recent studies have as-
 785 sociated the N₂O trend dipole discussed in the previous section with a southward shift
 786 of the circulation pattern, which in turn is related to the impact of mixing on the BDC
 787 changes (Stiller et al., 2017; Ploeger et al., 2019). Our results with N₂O from ERA5 con-
 788 firm the role of mixing processes above the southern mid-latitudes in determining changes
 789 in the N₂O abundances, and indirectly support the hypothesis of the southward shift of
 790 the circulation as a contribution to the dipole structure.

791 This qualitative analysis suggests that, within the N₂O TEM framework, changes
 792 in the residual circulation have a stronger impact on the direct N₂O trends compared
 793 to those in mixing. However, the ERA5 simulation also delivers significant N₂O changes
 794 due to mixing that are consistent with previous studies using ECMWF reanalyses and
 795 that can be associated to the hemispheric asymmetry in the direct N₂O trends simulated
 796 by ERA5.

797 6 Summary and Conclusions

798 We have evaluated the stratospheric N₂O columns (12-40 km) and their decadal
 799 (2005-2018) rates of change in two versions of WACCM: WACCM-REFC1 (version 4)
 800 and WACCM-REFD1 (version 6). We compared those changes with ground-based ob-
 801 servations at four ground-based FTIR stations: Lauder (45°S), Wollongong (34°S), Izaña
 802 (28°N) and Jungfraujoch (46°N), with space-borne measurements from ACE-FTS, and
 803 with the output of the BASCOE CTM driven by four modern reanalyses: ERAI, ERA5,
 804 JRA55 and MERRA2. We also studied the latitudinal and vertical distributions of these
 805 trends of the N₂O mixing ratios from model output and satellite measurements, both
 806 in the observation and model space. Also, we use the Transformed Eulerian Mean (TEM)
 807 budget to investigate further the decadal trends in the BASCOE CTM driven by ERA5
 808 and in WACCM-REFD1.

809 The comparison of the stratospheric N₂O columns reveals a good agreement above
 810 Wollongong, and Lauder to a lesser extent, and larger differences above Jungfraujoch and
 811 Izaña. The trends in the stratospheric N₂O columns obtained from FTIR are larger in
 812 the SH compared to the NH, which is consistent with hemispherical differences in trends
 813 of stratospheric tracers measured at FTIR stations over the past decade (Strahan et al.,
 814 2020; Prignon et al., 2021). This hemispheric asymmetry is present in the ECMWF re-
 815 analyses but is weaker in WACCM. We find that the decadal trends in the stratospheric
 816 N₂O columns are consistently positive in all cases except for ACE-FTS observations above
 817 Jungfraujoch. However, the vertical resolution of the FTIR retrievals above the NH for
 818 N₂O limits our analysis to one stratospheric column, hence (in this analysis) the detec-
 819 tion of potentially negative N₂O trends in the mid-stratosphere is hindered by the large
 820 N₂O increase in the lowermost stratosphere which arises from its continuous increase at
 821 the surface.

822 Global and vertically resolved trends of N₂O volume mixing ratios provide a more
 823 detailed picture compared to the stratospheric N₂O columns obtained from FTIR mea-
 824 surements. The ACE-FTS measurements show a meridional dipole in the N₂O trends
 825 in the mid-lower stratosphere, with negative values in the NH mid-latitudes and posi-
 826 tive values in the SH. When applying the temporal and spatial sampling of ACE-FTS
 827 on model datasets, ERAI and ERA5 compare best with the satellite measurements while
 828 the other reanalyses and WACCM do not reproduce the meridional dipole in the mid-
 829 lower stratosphere as clearly as the ECMWF reanalyses. However, this application of
 830 the irregular sampling of ACE-FTS to the model output consistently enhances the N₂O
 831 trends, both positive and negative. Using continuous time sampling on native model grids,
 832 ERAI, and ERA5 to a lesser extent, still simulate the meridional dipole in the N₂O trends,
 833 consistently with a large number of modeling studies using both idealized and real trac-
 834 ers (e.g., Chabrilat et al., 2018; Prignon et al., 2021; Ploeger & Garny, 2022), but MERRA2,
 835 JRA55 and both WACCM versions fail to reproduce the meridional dipole. The inher-
 836 ently limited spatial and temporal sampling of ACE-FTS, and its effect on N₂O trends,
 837 highlight the necessity to carry out the N₂O trend analysis discussed here using a satel-
 838 lite instrument with a more regular coverage. To this end, MLS is a very good candi-
 839 date, once its drift in the N₂O retrievals will be corrected.

840 Concerning the WACCM simulations, the too weak hemispheric asymmetries in
 841 the trends of the stratospheric N₂O columns and volume mixing ratios highlights small
 842 inter-hemispheric differences in the stratospheric transport. However, the adjusted parametriza-
 843 tion of gravity waves in version 6 of WACCM improves the trends in N₂O volume mix-
 844 ing ratios above the southern mid-latitudes compared to its version 4. This highlights
 845 the importance of the parametrization of the gravity waves for a correct reproduction
 846 of trends in long-lived tracers in the SH in WACCM. Therefore, we emphasize that mod-
 847 eling groups should continue their efforts in improving the horizontal resolution and ad-
 848 justing the gravity waves parametrization in CCMs.

849 We carried out two sensitivity tests using the BASCOE CTM driven by ERA5: one
 850 keeping N₂O constant at the surface with time-dependent dynamics (cst-N₂O), and the
 851 other using fixed dynamics with increasing N₂O at the surface (cst-dyn). The cst-N₂O
 852 experiment confirms that the extratropical N₂O trends in the mid-lower stratosphere are
 853 due to the impact of changes in the stratospheric transport. As expected, the cst-dyn
 854 simulation shows that N₂O increases everywhere, but the trend over 2005-2018 is not
 855 significantly positive in the NH mid-stratosphere. From these sensitivity tests with ERA5,
 856 we confirm that the hemispheric asymmetry of the decadal N₂O trends arises from decadal
 857 changes in the transport strength in combination with structural changes of the trans-
 858 port pattern. For the 2005-2018 period and in the 20-50 hPa layer, the hemispheric asym-
 859 metry in the significance of these trends arises from the larger dynamical variability which
 860 is found in the northern extratropics on shorter timescales, i.e. within one QBO cycle.

861 We found a strong impact of transport on the stratospheric trends of N₂O volume
 862 mixing ratios for the ERA5 simulations and large differences between ERA5 and WACCM-
 863 REFD1. This prompted us to study the TEM budget of N₂O in these two datasets, in
 864 order to separate the possible impacts of the residual circulation and mixing. For both
 865 datasets, the analysis of the TEM budget reveals positive N₂O changes in the tropical
 866 mid-high stratosphere and negative changes in the northern extratropical lower strato-
 867 sphere, as a result of enhanced tropical upwelling and extratropical downwelling, respec-
 868 tively. This is in agreement with the acceleration of the advective part of the BDC over
 869 this relatively short period both in models (Butchart, 2014) and reanalyses (Ploeger et
 870 al., 2019). For the ERA5 simulation, the positive N₂O trend above the southern mid-
 871 latitudes (part of the meridional dipole) can be due to the impact of changes in resolved
 872 mixing, which is consistent with previous studies, both using Age of Air (AoA, Ploeger
 873 et al., 2015) and N₂O (Stiller et al., 2017).

874 Using a measurable tracer for stratospheric transport studies allows direct com-
875 parisons with observations. The rate of change of N₂O at the surface is well-known and
876 approximately linear and the chemical losses are limited to the higher stratosphere. In
877 theory, this relatively simple chemistry, combined with its long life, makes N₂O a very
878 good tracer for stratospheric transport studies. Unfortunately, no ideal observational dataset
879 currently exists for N₂O-based investigations such as the present study: FTIR observa-
880 tions generally lack adequate vertical resolution, the N₂O product from the latest MLS
881 version suffers from an unrealistic drift, and ACE-FTS has poor spatial and temporal
882 sampling. Here, we showed how model studies of N₂O trends still provide new insights
883 about the BDC and its changes thanks to properly taking into account the ACE-FTS
884 sampling, complementary sensitivity tests, and the TEM analysis. In particular, the im-
885 provements in version 6 of WACCM compared to version 4 highlight that the next-generation
886 CCMs can potentially reach the quality of the reanalyses in terms of decadal changes
887 of long-lived tracers in the stratosphere. Despite the shortcomings of the TEM approach,
888 i.e., the difficulty of closing its budget, its combination with sensitivity tests provides new
889 insights on transport changes and their impacts on the composition of the stratosphere.
890 This approach could be extended to other tracers that are both measured and modeled
891 - e.g., carbon monoxide, methane, and inorganic fluorine.

892 Open Research

893 The WACCM and BASCOE CTM data used for the N₂O trends and TEM com-
894 parisons in the study are available at the BIRA-IASB repository ([http://repository](http://repository.aeronomie.be)
895 [.aeronomie.be](http://repository.aeronomie.be)) via <https://dx.doi.org/10.18758/71021071> with CC BY license (Minganti
896 & Errera, 2022). FTIR data at the various stations are available at [https://www-air](https://www-air.larc.nasa.gov/pub/NDACC/PUBLIC/stations/)
897 [.larc.nasa.gov/pub/NDACC/PUBLIC/stations/](https://www-air.larc.nasa.gov/pub/NDACC/PUBLIC/stations/). ACE-FTS data are available at [https://](https://database.scisat.ca/level2/ace.v4.1/display_data.php)
898 database.scisat.ca/level2/ace.v4.1/display_data.php. ERA5 data are available
899 at <https://cds.climate.copernicus.eu/>. ERA-Interim data are available at [https://](https://apps.ecmwf.int/datasets/)
900 apps.ecmwf.int/datasets/. JRA-55 data are available at <https://rda.ucar.edu/>.
901 MERRA2 data are available at <https://disc.gsfc.nasa.gov/datasets/>. The DLM
902 source code is available at <https://doi.org/10.5281/zenodo.2660704>.

903 Acknowledgments

904 We thank P. Bernath for his leadership of the ACE mission, which is supported by the
905 Canadian Space Agency. Measurements at Lauder are core-funded by the National In-
906 stitute of Water and Atmospheric Research Ltd. (NIWA) through New Zealand’s Min-
907 istry of Business, Innovation and Employment Strategic Science Investment Fund. The
908 ULiège team is grateful to the International Foundation High Altitude Research Stations
909 Jungfrauoch and Gornergrat (HFSJG, Bern) for supporting the facilities needed to per-
910 form the FTIR observations at Jungfrauoch. Funding via Helmholtz ATMO programme
911 has enabled the sustained NDACC FTIR activities at Izaña since the late 1990s. In ad-
912 dition, the Izaña NDACC FTIR observations strongly rely on the support (facilities and
913 operational activities) of the Izaña Atmospheric Research Centre of the Spanish Weather
914 Service (AEMET), with lead contributions of O. E. García. D. Minganti and M. Prignon
915 were financially supported by the Fonds de la Recherche Scientifique (F.R.S.-FNRS, Brus-
916 sels) through the ACCROSS research project (Grant no. PDR.T.0040.16). The Univer-
917 sity of Liège contribution was further supported by the GAW-CH program of MeteoSwiss
918 and by the F.R.S.-FNRS Grant no J.0126.21. E. Mahieu is a senior research associate
919 with the F.R.S.-FNRS. D. Kinnison was funded in part by National Aeronautics and Space
920 Administration (NASA) grant (NNH19ZDA001N-AURAST). This research was enabled
921 by the computational and storage resources of NCAR’s Computational and Information
922 Systems Laboratory (CISL), sponsored by the NSF. Cheyenne: HPE/SGI ICE XA Sys-
923 tem (NCAR Community Computing). Boulder, CO: National Center for Atmospheric
924 Research. <https://doi.org/10.5065/D6RX99HX>.

References

- 925
- 926 Abalos, M., Calvo, N., Benito-Barca, S., Garny, H., Hardiman, S. C., Lin, P., ...
 927 others (2021). The Brewer-Dobson circulation in CMIP6. *Atmospheric Chem-*
 928 *istry and Physics Discussions*, 1–27.
- 929 Abalos, M., Legras, B., Ploeger, F., & Randel, W. J. (2015). Evaluating the advective
 930 Brewer-Dobson circulation in three reanalyses for the period 1979–2012.
 931 *Journal of Geophysical Research: Atmospheres*, 120(15), 7534–7554.
- 932 Abalos, M., Orbe, C., Kinnison, D. E., Plummer, D., Oman, L. D., Jöckel, P., ...
 933 others (2020). Future trends in stratosphere-to-troposphere transport in CCM1
 934 models. *Atmospheric chemistry and physics*, 20(11), 6883–6901.
- 935 Abalos, M., Polvani, L., Calvo, N., Kinnison, D., Ploeger, F., Randel, W., &
 936 Solomon, S. (2019). New insights on the impact of ozone-depleting sub-
 937 stances on the Brewer-Dobson circulation. *Journal of Geophysical Research:*
 938 *Atmospheres*, 124(5), 2435–2451.
- 939 Abalos, M., Randel, W., Kinnison, D., & Serrano, E. (2013). Quantifying tracer
 940 transport in the tropical lower stratosphere using WACCM. *Atmos. Chem.*
 941 *Phys*, 13(10), 591–10.
- 942 Alexander, M. J., Liu, C. C., Bacmeister, J., Bramberger, M., Hertzog, A., &
 943 Richter, J. H. (2021). Observational validation of parameterized gravity waves
 944 from tropical convection in the whole atmosphere community climate model.
 945 *Journal of Geophysical Research: Atmospheres*, 126(7), e2020JD033954.
 946 Retrieved from [https://agupubs.onlinelibrary.wiley.com/doi/abs/](https://agupubs.onlinelibrary.wiley.com/doi/abs/10.1029/2020JD033954)
 947 [10.1029/2020JD033954](https://doi.org/10.1029/2020JD033954) (e2020JD033954) doi: [https://](https://doi.org/10.1029/2020JD033954)
 948 doi.org/10.1029/2020JD033954
- 949 Alsing, J. A. (2019). dlmrc: Dynamical linear model regression for atmospheric
 950 time-series analysis. *Journal of Open Source Software*, 4(37), 1157.
- 951 Andrews, A., Boering, K., Daube, B., Wofsy, S., Loewenstein, M., Jost, H., ... oth-
 952 ers (2001). Mean ages of stratospheric air derived from in situ observations of
 953 CO₂, CH₄, and N₂O. *Journal of Geophysical Research: Atmospheres*, 106(D23),
 954 32295–32314.
- 955 Andrews, D., Holton, J. R., & Leovy, C. B. (1987). *Middle atmosphere dynamics*
 956 (No. 40). Academic press.
- 957 Angelbratt, J., Mellqvist, J., Blumenstock, T., Borsdorff, T., Brohede, S.,
 958 Duchatelet, P., ... Urban, J. (2011). A new method to detect long term
 959 trends of methane (CH₄) and nitrous oxide (N₂O) total columns mea-
 960 sured within the NDACC ground-based high resolution solar FTIR net-
 961 work. *Atmospheric Chemistry and Physics*, 11(13), 6167–6183. Retrieved
 962 from <https://acp.copernicus.org/articles/11/6167/2011/> doi:
 963 [10.5194/acp-11-6167-2011](https://doi.org/10.5194/acp-11-6167-2011)
- 964 Bader, W., Bovy, B., Conway, S., Strong, K., Smale, D., Turner, A. J., ... Mahieu,
 965 E. (2017). The recent increase of atmospheric methane from 10 years of
 966 ground-based NDACC FTIR observations since 2005. *Atmospheric Chemistry and*
 967 *Physics*, 17(3), 2255–2277. Retrieved from [https://acp.copernicus.org/](https://acp.copernicus.org/articles/17/2255/2017/)
 968 [articles/17/2255/2017/](https://doi.org/10.5194/acp-17-2255-2017) doi: [10.5194/acp-17-2255-2017](https://doi.org/10.5194/acp-17-2255-2017)
- 969 Baldwin, M., Gray, L., Dunkerton, T., Hamilton, K., Haynes, P., Randel, W., ...
 970 others (2001). The quasi-biennial oscillation. *Reviews of Geophysics*, 39(2),
 971 179–229.
- 972 Ball, W. T., Alsing, J., Mortlock, D. J., Rozanov, E. V., Tummon, F., & Haigh,
 973 J. D. (2017). Reconciling differences in stratospheric ozone composites.
 974 *Atmospheric Chemistry and Physics*, 17(20), 12269–12302. Retrieved
 975 from <https://acp.copernicus.org/articles/17/12269/2017/> doi:
 976 [10.5194/acp-17-12269-2017](https://doi.org/10.5194/acp-17-12269-2017)
- 977 Ball, W. T., Alsing, J., Mortlock, D. J., Staehelin, J., Haigh, J. D., Peter, T., ...
 978 Rozanov, E. V. (2018). Evidence for a continuous decline in lower strato-
 979 spheric ozone offsetting ozone layer recovery. *Atmospheric Chemistry and*

- 980 *Physics*, 18(2), 1379–1394. Retrieved from [https://acp.copernicus.org/](https://acp.copernicus.org/articles/18/1379/2018/)
 981 [articles/18/1379/2018/](https://acp.copernicus.org/articles/18/1379/2018/) doi: 10.5194/acp-18-1379-2018
- 982 Bernath, P. (2017). The atmospheric chemistry experiment (ACE). *Journal of Quantitative Spectroscopy and Radiative Transfer*, 186, 3–16. Re-
 983 trieved from [https://www.sciencedirect.com/science/article/pii/](https://www.sciencedirect.com/science/article/pii/S0022407316300176)
 984 [S0022407316300176](https://www.sciencedirect.com/science/article/pii/S0022407316300176) (Satellite Remote Sensing and Spectroscopy: Joint ACE-
 985 Odin Meeting, October 2015) doi: <https://doi.org/10.1016/j.jqsrt.2016.04.006>
- 986 Bernath, P., Crouse, J., Hughes, R., & Boone, C. (2021). The Atmospheric Chem-
 987 istry Experiment Fourier transform spectrometer (ACE-FTS) version 4.1
 988 retrievals: Trends and seasonal distributions. *Journal of Quantitative Spec-*
 989 *troscopy and Radiative Transfer*, 259, 107409.
- 990 Bernath, P., McElroy, C. T., Abrams, M. C., Boone, C. D., Butler, M., Camy-
 991 Peyret, C., ... Zou, J. (2005). Atmospheric chemistry experiment (ACE): Mis-
 992 sion overview. *Geophysical Research Letters*, 32(15). Retrieved from [https://](https://agupubs.onlinelibrary.wiley.com/doi/abs/10.1029/2005GL022386)
 993 agupubs.onlinelibrary.wiley.com/doi/abs/10.1029/2005GL022386 doi:
 994 <https://doi.org/10.1029/2005GL022386>
- 995 Bernath, P., Steffen, J., Crouse, J., & Boone, C. (2020). Sixteen-year trends
 996 in atmospheric trace gases from orbit. *Journal of Quantitative Spec-*
 997 *troscopy and Radiative Transfer*, 253, 107178. Retrieved from [https://](https://www.sciencedirect.com/science/article/pii/S0022407320302958)
 998 www.sciencedirect.com/science/article/pii/S0022407320302958 doi:
 999 <https://doi.org/10.1016/j.jqsrt.2020.107178>
- 1000 Brewer, A. (1949). Evidence for a world circulation provided by the measurements
 1001 of helium and water vapour distribution in the stratosphere. *Quarterly Journal*
 1002 *of the Royal Meteorological Society*, 75(326), 351–363.
- 1003 Butchart, N. (2014). The Brewer-Dobson circulation. *Reviews of Geophysics*, 52(2),
 1004 157–184. Retrieved from [https://agupubs.onlinelibrary.wiley.com/doi/](https://agupubs.onlinelibrary.wiley.com/doi/abs/10.1002/2013RG000448)
 1005 [abs/10.1002/2013RG000448](https://agupubs.onlinelibrary.wiley.com/doi/abs/10.1002/2013RG000448) doi: <https://doi.org/10.1002/2013RG000448>
- 1006 Butchart, N., & Scaife, A. A. (2001). Removal of chlorofluorocarbons by increased
 1007 mass exchange between the stratosphere and troposphere in a changing cli-
 1008 mate. *Nature*, 410(6830), 799–802.
- 1009 Chabrillat, S., Vigouroux, C., Christophe, Y., Engel, A., Errera, Q., Minganti, D.,
 1010 ... Mahieu, E. (2018). Comparison of mean age of air in five reanalyses using
 1011 the BASCOE transport model. *Atmospheric Chemistry and Physics*, 18(19),
 1012 14715–14735.
- 1013 Charney, J. G., & Drazin, P. G. (1961). Propagation of planetary-scale disturbances
 1014 from the lower into the upper atmosphere. *Journal of Geophysical Research*,
 1015 66(1), 83–109.
- 1016 Danabasoglu, G., Lamarque, J.-F., Bacmeister, J., Bailey, D., DuVivier, A., Ed-
 1017 wards, J., ... others (2020). The community earth system model version 2
 1018 (CESM2). *Journal of Advances in Modeling Earth Systems*, 12(2).
- 1019 Darrag, M., Jin, S., Calabia, A., & Samy, A. (2022). Determination of tropical belt
 1020 widening using multiple gnss radio occultation measurements. *Annales Geo-*
 1021 *physicae*, 40(3), 359–377. Retrieved from [https://angeo.copernicus.org/](https://angeo.copernicus.org/articles/40/359/2022/)
 1022 [articles/40/359/2022/](https://angeo.copernicus.org/articles/40/359/2022/) doi: 10.5194/angeo-40-359-2022
- 1023 Dee, D. P., Uppala, S., Simmons, A., Berrisford, P., Poli, P., Kobayashi, S., ... oth-
 1024 ers (2011). The ERA-interim reanalysis: Configuration and performance of the
 1025 data assimilation system. *Quarterly Journal of the royal meteorological society*,
 1026 137(656), 553–597.
- 1027 De Mazière, M., Thompson, A. M., Kurylo, M. J., Wild, J. D., Bernhard, G., Blu-
 1028 menstock, T., ... others (2018). The Network for the Detection of Atmo-
 1029 spheric Composition Change (NDACC): history, status and perspectives.
 1030 *Atmospheric Chemistry and Physics*, 18(7), 4935–4964.
- 1031 de Wit, T. D., Bruinsma, S., & Shibasaki, K. (2014). Synoptic radio observations as
 1032 proxies for upper atmosphere modelling. *Journal of Space Weather and Space*
 1033 *Climate*, 4, A06.

- 1035 Dhomse, S. S., Kinnison, D., Chipperfield, M. P., Salawitch, R. J., Cionni, I.,
 1036 Hegglin, M. I., ... Zeng, G. (2018). Estimates of ozone return dates from
 1037 Chemistry-Climate Model Initiative simulations. *Atmospheric Chemistry and*
 1038 *Physics*, *18*(11), 8409–8438. Retrieved from [https://acp.copernicus.org/](https://acp.copernicus.org/articles/18/8409/2018/)
 1039 [articles/18/8409/2018/](https://acp.copernicus.org/articles/18/8409/2018/) doi: 10.5194/acp-18-8409-2018
- 1040 Diallo, M., Ern, M., & Ploeger, F. (2021). The advective brewer–dobson circulation
 1041 in the era5 reanalysis: climatology, variability, and trends. *Atmospheric Chem-*
 1042 *istry and Physics*, *21*(10), 7515–7544.
- 1043 Diallo, M., Legras, B., & Chédin, A. (2012). Age of stratospheric air in the era-
 1044 interim. *Atmospheric Chemistry and Physics*, *12*(24), 12133–12154.
- 1045 Dietmüller, S., Eichinger, R., Garny, H., Birner, T., Boenisch, H., Pitari, G., ... oth-
 1046 ers (2018). Quantifying the effect of mixing on the mean age of air in ccmval-2
 1047 and ccmi-1 models. *Atmospheric Chemistry and Physics*, *18*(9), 6699–6720.
- 1048 Dietmüller, S., Garny, H., Plöger, F., Jöckel, P., & Cai, D. (2017). Effects of mix-
 1049 ing on resolved and unresolved scales on stratospheric age of air. *Atmospheric*
 1050 *chemistry and physics*, *17*(12), 7703–7719.
- 1051 Dobson, G. M. B. (1956). Origin and distribution of the polyatomic molecules in the
 1052 atmosphere. *Proceedings of the Royal Society of London. Series A. Mathematical*
 1053 *and Physical Sciences*, *236*(1205), 187–193.
- 1054 Dobson, G. M. B., Harrison, D., & Lawrence, J. (1929). Measurements of the
 1055 amount of ozone in the earth's atmosphere and its relation to other geo-
 1056 physical conditions. 2014part iii. *Proceedings of the Royal Society of Lon-*
 1057 *don. Series A, Containing Papers of a Mathematical and Physical Character*,
 1058 *122*(790), 456–486.
- 1059 Dubé, K., Randel, W., Bourassa, A., Zawada, D., McLinden, C., & Degenstein,
 1060 D. (2020). Trends and variability in stratospheric nox derived from
 1061 merged sage ii and osiris satellite observations. *Journal of Geophysical Re-*
 1062 *search: Atmospheres*, *125*(7), e2019JD031798. Retrieved from [https://](https://agupubs.onlinelibrary.wiley.com/doi/abs/10.1029/2019JD031798)
 1063 agupubs.onlinelibrary.wiley.com/doi/abs/10.1029/2019JD031798
 1064 (e2019JD031798 10.1029/2019JD031798) doi: [https://doi.org/10.1029/](https://doi.org/10.1029/2019JD031798)
 1065 [2019JD031798](https://doi.org/10.1029/2019JD031798)
- 1066 Durbin, J., & Koopman, S. J. (2012). *Time series analysis by state space methods*.
 1067 Oxford university press.
- 1068 Eichinger, R., Dietmüller, S., Garny, H., Šácha, P., Birner, T., Bönisch, H., ... oth-
 1069 ers (2019). The influence of mixing on the stratospheric age of air changes in
 1070 the 21st century. *Atmospheric chemistry and physics*, *19*(2), 921–940.
- 1071 Eichinger, R., & Šácha, P. (2020). Overestimated acceleration of the advective
 1072 Brewer–Dobson circulation due to stratospheric cooling. *Quarterly Journal of*
 1073 *the Royal Meteorological Society*, *146*(733), 3850–3864.
- 1074 Engel, A., Bönisch, H., Ullrich, M., Sitals, R., Membrive, O., Danis, F., &
 1075 Crevoisier, C. (2017). Mean age of stratospheric air derived from AirCore
 1076 observations. *Atmospheric Chemistry and Physics*, *17*(11), 6825–6838.
- 1077 Engel, A., Möbius, T., Bönisch, H., Schmidt, U., Heinz, R., Levin, I., ... others
 1078 (2009). Age of stratospheric air unchanged within uncertainties over the past
 1079 30 years. *Nature Geoscience*, *2*(1), 28–31.
- 1080 Errera, Q., Chabrillat, S., Christophe, Y., Deboscher, J., Hubert, D., Lahoz, W.,
 1081 ... Walker, K. (2019). Technical note: Reanalysis of Aura MLS Chemical
 1082 Observations. *Atmospheric Chemistry and Physics Discussions*, *2019*, 1–60.
 1083 Retrieved from <https://www.atmos-chem-phys-discuss.net/acp-2019-530/>
 1084 doi: 10.5194/acp-2019-530
- 1085 Eyring, V., Bony, S., Meehl, G. A., Senior, C. A., Stevens, B., Stouffer, R. J., &
 1086 Taylor, K. E. (2016). Overview of the coupled model intercomparison project
 1087 phase 6 (cmip6) experimental design and organization. *Geoscientific Model*
 1088 *Development*, *9*(5), 1937–1958.
- 1089 Eyring, V., Lamarque, J.-F., Hess, P., Arfeuille, F., Bowman, K., Chipperfield, M. P.,

- 1090 ... others (2013). Overview of igac/sparc chemistry-climate model initia-
 1091 tive (ccmi) community simulations in support of upcoming ozone and climate
 1092 assessments. *SPARC newsletter*, 40(Januar), 48–66.
- 1093 Fritsch, F., Garny, H., Engel, A., Bönisch, H., & Eichinger, R. (2020). Sensitiv-
 1094 ity of age of air trends to the derivation method for non-linear increasing
 1095 inert SF₆. *Atmospheric Chemistry and Physics*, 20(14), 8709–8725. Re-
 1096 trieved from <https://www.atmos-chem-phys.net/20/8709/2020/> doi:
 1097 10.5194/acp-20-8709-2020
- 1098 Froidevaux, L., Kinnison, D. E., Wang, R., Anderson, J., & Fuller, R. A. (2019).
 1099 Evaluation of CESM1 (WACCM) free-running and specified dynamics at-
 1100 mospheric composition simulations using global multispecies satellite data
 1101 records. *Atmospheric Chemistry and Physics*, 19(7), 4783–4821. Re-
 1102 trieved from <https://acp.copernicus.org/articles/19/4783/2019/> doi:
 1103 10.5194/acp-19-4783-2019
- 1104 Fu, Q., Lin, P., Solomon, S., & Hartmann, D. (2015). Observational evidence of
 1105 strengthening of the Brewer–Dobson circulation since 1980. *Journal of Geo-*
 1106 *physical Research: Atmospheres*, 120(19), 10–214.
- 1107 Fujiwara, M., Wright, J. S., Manney, G. L., Gray, L. J., Anstey, J., Birner, T., ...
 1108 others (2017). Introduction to the SPARC Reanalysis Intercomparison Project
 1109 (S-RIP) and overview of the reanalysis systems. *Atmospheric Chemistry and*
 1110 *Physics*, 17(2), 1417–1452.
- 1111 Galytska, E., Rozanov, A., Chipperfield, M. P., Dhomse, Weber, M., Arosio, C., ...
 1112 Burrows, J. P. (2019). Dynamically controlled ozone decline in the tropi-
 1113 cal mid-stratosphere observed by SCIAMACHY. *Atmospheric Chemistry and*
 1114 *Physics*, 19(2), 767–783. Retrieved from [https://www.atmos-chem-phys.net/](https://www.atmos-chem-phys.net/19/767/2019/)
 1115 [19/767/2019/](https://www.atmos-chem-phys.net/19/767/2019/) doi: 10.5194/acp-19-767-2019
- 1116 García, O. E., Schneider, M., Sepúlveda, E., Hase, F., Blumenstock, T., Cuevas, E.,
 1117 ... López, C. (2021). Twenty years of ground-based NDACC FTIR spec-
 1118 trometry at Izaña Observatory – overview and long-term comparison to other
 1119 techniques. *Atmospheric Chemistry and Physics*, 21(20), 15519–15554. Re-
 1120 trieved from <https://acp.copernicus.org/articles/21/15519/2021/> doi:
 1121 10.5194/acp-21-15519-2021
- 1122 Garcia, R. R., Randel, W. J., & Kinnison, D. E. (2011). On the determination of
 1123 age of air trends from atmospheric trace species. *Journal of the Atmospheric*
 1124 *Sciences*, 68(1), 139–154.
- 1125 Garcia, R. R., Smith, A. K., Kinnison, D. E., de la Cámara, A., & Murphy, D. J.
 1126 (2017). Modification of the Gravity Wave Parameterization in the Whole
 1127 Atmosphere Community Climate Model: Motivation and Results. *Journal*
 1128 *of the Atmospheric Sciences*, 74(1), 275 - 291. Retrieved from [https://](https://journals.ametsoc.org/view/journals/atsc/74/1/jas-d-16-0104.1.xml)
 1129 journals.ametsoc.org/view/journals/atsc/74/1/jas-d-16-0104.1.xml
 1130 doi: 10.1175/JAS-D-16-0104.1
- 1131 Garny, H., Birner, T., Bönisch, H., & Bunzel, F. (2014). The effects of mixing on
 1132 age of air. *Journal of Geophysical Research: Atmospheres*, 119(12), 7015–
 1133 7034.
- 1134 Gelaro, R., McCarty, W., Suárez, M. J., Todling, R., Molod, A., Takacs, L., ...
 1135 others (2017). The modern-era retrospective analysis for research and applica-
 1136 tions, version 2 (MERRA-2). *Journal of Climate*, 30(14), 5419–5454.
- 1137 Gettelman, A., Mills, M., Kinnison, D., Garcia, R., Smith, A., Marsh, D., ... oth-
 1138 ers (2019). The whole atmosphere community climate model version 6
 1139 (WACCM6). *Journal of Geophysical Research: Atmospheres*, 124(23), 12380–
 1140 12403.
- 1141 Griffith, D. W. T., Deutscher, N. M., Caldow, C., Kettlewell, G., Riggenbach, M.,
 1142 & Hammer, S. (2012). A Fourier transform infrared trace gas and isotope
 1143 analyser for atmospheric applications. *Atmospheric Measurement Techniques*,
 1144 5(10), 2481–2498. Retrieved from <https://amt.copernicus.org/articles/>

- 1145 5/2481/2012/ doi: 10.5194/amt-5-2481-2012
- 1146 Haenel, F. J., Stiller, G. P., von Clarmann, T., Funke, B., Eckert, E., Glatthor, N.,
 1147 ... Reddman, T. (2015). Reassessment of MIPAS age of air trends and
 1148 variability. *Atmospheric Chemistry and Physics*, 15(22), 13161–13176. Re-
 1149 trieved from <https://acp.copernicus.org/articles/15/13161/2015/> doi:
 1150 10.5194/acp-15-13161-2015
- 1151 Hall, T. M., & Plumb, R. A. (1994). Age as a diagnostic of stratospheric transport.
 1152 *Journal of Geophysical Research: Atmospheres*, 99(D1), 1059–1070.
- 1153 Han, Y., Tian, W., Chipperfield, M. P., Zhang, J., Wang, F., Sang, W., ... Tian,
 1154 H. (2019). Attribution of the Hemispheric Asymmetries in Trends of Strato-
 1155 spheric Trace Gases Inferred From Microwave Limb Sounder (MLS) Measure-
 1156 ments. *Journal of Geophysical Research: Atmospheres*, 124(12), 6283–6293.
 1157 Retrieved from [https://agupubs.onlinelibrary.wiley.com/doi/abs/](https://agupubs.onlinelibrary.wiley.com/doi/abs/10.1029/2018JD029723)
 1158 [10.1029/2018JD029723](https://doi.org/10.1029/2018JD029723) doi: <https://doi.org/10.1029/2018JD029723>
- 1159 Hardiman, S. C., Butchart, N., & Calvo, N. (2014). The morphology of the Brewer–
 1160 Dobson circulation and its response to climate change in CMIP5 simulations.
 1161 *Quarterly Journal of the Royal Meteorological Society*, 140(683), 1958–1965.
- 1162 Hardiman, S. C., Lin, P., Scaife, A. A., Dunstone, N. J., & Ren, H.-L. (2017). The
 1163 influence of dynamical variability on the observed Brewer–Dobson circulation
 1164 trend. *Geophysical Research Letters*, 44(6), 2885–2892.
- 1165 Harrison, J. J., Chipperfield, M. P., Boone, C. D., Dhomse, S. S., Bernath, P. F.,
 1166 Froidevaux, L., ... Russell III, J. (2016). Satellite observations of stratospheric
 1167 hydrogen fluoride and comparisons with SLIMCAT calculations. *Atmospheric*
 1168 *Chemistry and Physics*, 16(16), 10501–10519.
- 1169 Hegglin, M., Plummer, D., Shepherd, T., Scinocca, J., Anderson, J., Froidevaux,
 1170 L., ... others (2014). Vertical structure of stratospheric water vapour trends
 1171 derived from merged satellite data. *Nature Geoscience*, 7(10), 768–776.
- 1172 Hersbach, H., Bell, B., Berrisford, P., Hirahara, S., Hornyi, A., Muoz-Sabater, J.,
 1173 ... Thpaut, J.-N. (2020). The ERA5 global reanalysis. *Quarterly Journal*
 1174 *of the Royal Meteorological Society*, 146(730), 1999–2049. Retrieved from
 1175 <https://rmets.onlinelibrary.wiley.com/doi/abs/10.1002/qj.3803> doi:
 1176 <https://doi.org/10.1002/qj.3803>
- 1177 Holton, J. (2004). *An introduction to dynamic meteorology* (No. v. 1). Else-
 1178 vier Academic Press. Retrieved from [https://books.google.it/books?id=](https://books.google.it/books?id=fhW5oDv3EPsC)
 1179 [fhW5oDv3EPsC](https://books.google.it/books?id=fhW5oDv3EPsC)
- 1180 Holton, J., & Choi, W.-K. (1988). Transport circulation deduced from sams trace
 1181 species data. *Journal of Atmospheric Sciences*, 45(13), 1929–1939.
- 1182 Hurrell, J. W., Holland, M. M., Gent, P. R., Ghan, S., Kay, J. E., Kushner, P. J.,
 1183 ... others (2013). The community earth system model: a framework for col-
 1184 laborative research. *Bulletin of the American Meteorological Society*, 94(9),
 1185 1339–1360.
- 1186 Jin, J. J., Semeniuk, K., Beagley, S. R., Fomichev, V. I., Jonsson, A. I., McConnell,
 1187 J. C., ... Dupuy, E. (2009). Comparison of cmam simulations of carbon
 1188 monoxide (co), nitrous oxide (n₂o), and methane (ch₄) with observations from
 1189 odin/smr, ace-fs, and aura/mls. *Atmospheric Chemistry and Physics*, 9(10),
 1190 3233–3252. Retrieved from [https://acp.copernicus.org/articles/9/3233/](https://acp.copernicus.org/articles/9/3233/2009/)
 1191 [2009/](https://acp.copernicus.org/articles/9/3233/2009/) doi: 10.5194/acp-9-3233-2009
- 1192 Kobayashi, S., Ota, Y., Harada, Y., Ebata, A., Moriya, M., Onoda, H., ... others
 1193 (2015). The JRA-55 reanalysis: General specifications and basic characteris-
 1194 tics. *Journal of the Meteorological Society of Japan. Ser. II*, 93(1), 5–48.
- 1195 Kolonjari, F., Plummer, D. A., Walker, K. A., Boone, C. D., Elkins, J. W., Heg-
 1196 glin, M. I., ... Stiller, G. P. (2018). Assessing stratospheric transport in the
 1197 cmam30 simulations using ace-fs measurements. *Atmospheric Chemistry and*
 1198 *Physics*, 18(9), 6801–6828. Retrieved from [https://acp.copernicus.org/](https://acp.copernicus.org/articles/18/6801/2018/)
 1199 [articles/18/6801/2018/](https://acp.copernicus.org/articles/18/6801/2018/) doi: 10.5194/acp-18-6801-2018

- 1200 Kyrölä, E., Laine, M., Sofieva, V., Tamminen, J., Päivärinta, S.-M., Tukiainen, S.,
 1201 ... Thomason, L. (2013). Combined sage ii-gomos ozone profile data set for
 1202 1984–2011 and trend analysis of the vertical distribution of ozone. *Atmospheric*
 1203 *Chemistry and Physics*, *13*(21), 10645–10658.
- 1204 Laine, M., Latva-Pukkila, N., & Kyrölä, E. (2014). Analysing time-varying trends
 1205 in stratospheric ozone time series using the state space approach. *Atmospheric*
 1206 *Chemistry and Physics*, *14*(18), 9707–9725.
- 1207 Langerock, B., De Mazière, M., Hendrick, F., Vigouroux, C., Desmet, F., Dils, B., &
 1208 Niemeijer, S. (2015). Description of algorithms for co-locating and comparing
 1209 gridded model data with remote-sensing observations. *Geoscientific Model*
 1210 *Development*, *8*(3), 911–921. Retrieved from [https://gmd.copernicus.org/](https://gmd.copernicus.org/articles/8/911/2015/)
 1211 [articles/8/911/2015/](https://gmd.copernicus.org/articles/8/911/2015/) doi: 10.5194/gmd-8-911-2015
- 1212 Lin, P., & Fu, Q. (2013). Changes in various branches of the Brewer–Dobson circula-
 1213 tion from an ensemble of chemistry climate models. *Journal of Geophysical Re-*
 1214 *search: Atmospheres*, *118*(1), 73–84.
- 1215 Lin, S., & Rood, R. B. (1996). Multidimensional flux-form semi-lagrangian transport
 1216 schemes. *Monthly Weather Review*, *124*(9), 2046–2070.
- 1217 Lin, S.-J. (2004). A "vertically lagrangian" finite-volume dynamical core for global
 1218 models. *Monthly Weather Review*, *132*(10), 2293–2307.
- 1219 Linz, M., Plumb, R. A., Gupta, A., & Gerber, E. P. (2021). Stratospheric adiabatic
 1220 mixing rates derived from the vertical gradient of age of air. *Journal of Geo-*
 1221 *physical Research: Atmospheres*, *126*(21), e2021JD035199.
- 1222 Livesey, N. J., Read, W. G., Froidevaux, L., Lambert, A., Santee, M. L., Schwartz,
 1223 M. J., ... Nedoluha, G. E. (2021). Investigation and amelioration of long-term
 1224 instrumental drifts in water vapor and nitrous oxide measurements from the
 1225 aura microwave limb sounder (MLS) and their implications for studies of vari-
 1226 ability and trends. *Atmospheric Chemistry and Physics*, *21*(20), 15409–15430.
 1227 Retrieved from <https://acp.copernicus.org/articles/21/15409/2021/>
 1228 doi: 10.5194/acp-21-15409-2021
- 1229 Mahieu, E., Chipperfield, M., Notholt, J., Reddman, T., Anderson, J., Bernath, P.,
 1230 ... others (2014). Recent northern hemisphere stratospheric HCl increase due
 1231 to atmospheric circulation changes. *Nature*, *515*(7525), 104.
- 1232 Manney, G. L., & Hegglin, M. I. (2018). Seasonal and regional variations of long-
 1233 term changes in upper-tropospheric jets from reanalyses. *Journal of Climate*,
 1234 *31*(1), 423–448.
- 1235 Marsh, D. R., Mills, M. J., Kinnison, D. E., Lamarque, J.-F., Calvo, N., & Polvani,
 1236 L. M. (2013). Climate change from 1850 to 2005 simulated in cesm1(waccm).
 1237 *Journal of Climate*, *26*(19), 7372 - 7391. Retrieved from [https://journals](https://journals.ametsoc.org/view/journals/clim/26/19/jcli-d-12-00558.1.xml)
 1238 [.ametsoc.org/view/journals/clim/26/19/jcli-d-12-00558.1.xml](https://journals.ametsoc.org/view/journals/clim/26/19/jcli-d-12-00558.1.xml) doi:
 1239 10.1175/JCLI-D-12-00558.1
- 1240 Matthes, K., Marsh, D. R., Garcia, R. R., Kinnison, D. E., Sassi, F., & Walters, S.
 1241 (2010). Role of the qbo in modulating the influence of the 11 year solar cycle
 1242 on the atmosphere using constant forcings. *Journal of Geophysical Research:*
 1243 *Atmospheres*, *115*(D18).
- 1244 Meinshausen, M., Nicholls, Z. R. J., Lewis, J., Gidden, M. J., Vogel, E., Freund, M.,
 1245 ... Wang, R. H. J. (2020). The shared socio-economic pathway (ssp) green-
 1246 house gas concentrations and their extensions to 2500. *Geoscientific Model De-*
 1247 *velopment*, *13*(8), 3571–3605. Retrieved from [https://gmd.copernicus.org/](https://gmd.copernicus.org/articles/13/3571/2020/)
 1248 [articles/13/3571/2020/](https://gmd.copernicus.org/articles/13/3571/2020/) doi: 10.5194/gmd-13-3571-2020
- 1249 Meul, S., Dameris, M., Langematz, U., Abalichin, J., Kerschbaumer, A., Ku-
 1250 bin, A., & Oberlinder-Hayn, S. (2016). Impact of rising greenhouse
 1251 gas concentrations on future tropical ozone and UV exposure. *Geo-*
 1252 *physical Research Letters*, *43*(6), 2919-2927. Retrieved from [https://](https://agupubs.onlinelibrary.wiley.com/doi/abs/10.1002/2016GL067997)
 1253 agupubs.onlinelibrary.wiley.com/doi/abs/10.1002/2016GL067997 doi:
 1254 <https://doi.org/10.1002/2016GL067997>

- 1255 Meul, S., Langematz, U., Kröger, P., Oberländer-Hayn, S., & Jöckel, P. (2018). Fu-
 1256 ture changes in the stratosphere-to-troposphere ozone mass flux and the con-
 1257 tribution from climate change and ozone recovery. *Atmospheric Chemistry and*
 1258 *Physics*, *18*(10), 7721–7738. Retrieved from [https://acp.copernicus.org/](https://acp.copernicus.org/articles/18/7721/2018/)
 1259 [articles/18/7721/2018/](https://acp.copernicus.org/articles/18/7721/2018/) doi: 10.5194/acp-18-7721-2018
- 1260 Millán, L. F., Livesey, N. J., Santee, M. L., Neu, J. L., Manney, G. L., & Fuller,
 1261 R. A. (2016). Case studies of the impact of orbital sampling on stratospheric
 1262 trend detection and derivation of tropical vertical velocities: solar occultation
 1263 vs. limb emission sounding. *Atmospheric Chemistry and Physics*, *16*(18),
 1264 11521–11534. Retrieved from [https://acp.copernicus.org/articles/16/](https://acp.copernicus.org/articles/16/11521/2016/)
 1265 [11521/2016/](https://acp.copernicus.org/articles/16/11521/2016/) doi: 10.5194/acp-16-11521-2016
- 1266 Mills, M. J., Richter, J. H., Tilmes, S., Kravitz, B., MacMartin, D. G., Glanville,
 1267 A. A., ... Kinnison, D. E. (2017). Radiative and chemical response to inter-
 1268 active stratospheric sulfate aerosols in fully coupled cesm1(waccm). *Journal*
 1269 *of Geophysical Research: Atmospheres*, *122*(23), 13,061–13,078. Retrieved
 1270 from [https://agupubs.onlinelibrary.wiley.com/doi/abs/10.1002/](https://agupubs.onlinelibrary.wiley.com/doi/abs/10.1002/2017JD027006)
 1271 [2017JD027006](https://agupubs.onlinelibrary.wiley.com/doi/abs/10.1002/2017JD027006) doi: <https://doi.org/10.1002/2017JD027006>
- 1272 Minganti, D., Chabrilat, S., Christophe, Y., Errera, Q., Abalos, M., Prignon, M., ...
 1273 Mahieu, E. (2020). Climatological impact of the Brewer–Dobson circulation on
 1274 the N₂O budget in WACCM, a chemical reanalysis and a CTM driven by four
 1275 dynamical reanalyses. *Atmospheric Chemistry and Physics*, *20*(21), 12609–
 1276 12631. Retrieved from [https://acp.copernicus.org/articles/20/12609/](https://acp.copernicus.org/articles/20/12609/2020/)
 1277 [2020/](https://acp.copernicus.org/articles/20/12609/2020/) doi: 10.5194/acp-20-12609-2020
- 1278 Minganti, D., & Errera, Q. (2022). *Supplement for: N₂O rate of change as a di-*
 1279 *agnostic of the brewer-dobson circulation in the stratosphere* [dataset]. Royal
 1280 Belgian Institute for Space Aeronomy. Retrieved from [https://repository](https://repository.aeronomie.be/?doi=10.18758/71021071)
 1281 [.aeronomie.be/?doi=10.18758/71021071](https://repository.aeronomie.be/?doi=10.18758/71021071) doi: [https://dx.doi.org/10.18758/](https://dx.doi.org/10.18758/71021071)
 1282 [71021071](https://dx.doi.org/10.18758/71021071)
- 1283 Minschwaner, K., Su, H., & Jiang, J. H. (2016). The upward branch of the brewer-
 1284 dobson circulation quantified by tropical stratospheric water vapor and car-
 1285 bon monoxide measurements from the aura microwave limb sounder. *Jour-*
 1286 *nal of Geophysical Research: Atmospheres*, *121*(6), 2790–2804. Retrieved
 1287 from [https://agupubs.onlinelibrary.wiley.com/doi/abs/10.1002/](https://agupubs.onlinelibrary.wiley.com/doi/abs/10.1002/2015JD023961)
 1288 [2015JD023961](https://agupubs.onlinelibrary.wiley.com/doi/abs/10.1002/2015JD023961) doi: <https://doi.org/10.1002/2015JD023961>
- 1289 Monge-Sanz, B. M., Chipperfield, M. P., Dee, D. P., Simmons, A. J., & Uppala,
 1290 S. M. (2012). Improvements in the stratospheric transport achieved by a
 1291 chemistry transport model with ECMWF (re)analyses: identifying effects and
 1292 remaining challenges. *Quarterly Journal of the Royal Meteorological Society*,
 1293 *139*(672), 654–673. Retrieved from [https://rmets.onlinelibrary.wiley](https://rmets.onlinelibrary.wiley.com/doi/abs/10.1002/qj.1996)
 1294 [.com/doi/abs/10.1002/qj.1996](https://rmets.onlinelibrary.wiley.com/doi/abs/10.1002/qj.1996) doi: <https://doi.org/10.1002/qj.1996>
- 1295 Morgenstern, O., Hegglin, M. I., Rozanov, E., O’Connor, F. M., Abraham, N. L.,
 1296 Akiyoshi, H., ... Zeng, G. (2017). Review of the global models used within
 1297 phase 1 of the chemistry–climate model initiative (ccmi). *Geoscientific Model*
 1298 *Development*, *10*(2), 639–671. Retrieved from [https://gmd.copernicus.org/](https://gmd.copernicus.org/articles/10/639/2017/)
 1299 [articles/10/639/2017/](https://gmd.copernicus.org/articles/10/639/2017/) doi: 10.5194/gmd-10-639-2017
- 1300 Neale, R. B., Richter, J., Park, S., Lauritzen, P. H., Vavrus, S. J., Rasch, P. J., &
 1301 Zhang, M. (2013). The mean climate of the Community Atmosphere Model
 1302 (CAM4) in forced SST and fully coupled experiments. *Journal of Climate*,
 1303 *26*(14), 5150–5168.
- 1304 Nedoluha, G. E., Siskind, D. E., Lambert, A., & Boone, C. (2015). The decrease
 1305 in mid-stratospheric tropical ozone since 1991. *Atmospheric Chemistry and*
 1306 *Physics*, *15*(8), 4215–4224. Retrieved from [https://acp.copernicus.org/](https://acp.copernicus.org/articles/15/4215/2015/)
 1307 [articles/15/4215/2015/](https://acp.copernicus.org/articles/15/4215/2015/) doi: 10.5194/acp-15-4215-2015
- 1308 Oberländer-Hayn, S., Gerber, E. P., Abalichin, J., Akiyoshi, H., Kerschbaumer,
 1309 A., Kubin, A., ... Oman, L. D. (2016). Is the Brewer-Dobson circulation

- 1310 increasing or moving upward? *Geophysical Research Letters*, *43*(4), 1772-
 1311 1779. Retrieved from [https://agupubs.onlinelibrary.wiley.com/doi/abs/](https://agupubs.onlinelibrary.wiley.com/doi/abs/10.1002/2015GL067545)
 1312 [10.1002/2015GL067545](https://doi.org/10.1002/2015GL067545) doi: <https://doi.org/10.1002/2015GL067545>
- 1313 Pisoft, P., Sacha, P., Polvani, L. M., Añel, J. A., De La Torre, L., Eichinger, R., ...
 1314 others (2021). Stratospheric contraction caused by increasing greenhouse gases.
 1315 *Environmental Research Letters*, *16*(6), 064038.
- 1316 Ploeger, F., Abalos, M., Birner, T., Konopka, P., Legras, B., Müller, R., & Riese, M.
 1317 (2015). Quantifying the effects of mixing and residual circulation on trends of
 1318 stratospheric mean age of air. *Geophysical Research Letters*, *42*(6), 2047–2054.
- 1319 Ploeger, F., Diallo, M., Charlesworth, E., Konopka, P., Legras, B., Laube, J. C.,
 1320 ... Riese, M. (2021). The stratospheric Brewer–Dobson circulation inferred
 1321 from age of air in the ERA5 reanalysis. *Atmospheric Chemistry and Physics*,
 1322 *21*(11), 8393–8412.
- 1323 Ploeger, F., & Garny, H. (2022). Hemispheric asymmetries in recent changes in
 1324 the stratospheric circulation. *Atmospheric Chemistry and Physics*, *22*(8),
 1325 5559–5576.
- 1326 Ploeger, F., Legras, B., Charlesworth, E., Yan, X., Diallo, M., Konopka, P., ...
 1327 Riese, M. (2019). How robust are stratospheric age of air trends from different
 1328 reanalyses? *Atmospheric Chemistry and Physics*, *19*(9), 6085–6105.
- 1329 Plumb, R. A. (2002). Stratospheric transport. *Journal of the Meteorological Society*
 1330 *of Japan. Ser. II*, *80*(4B), 793–809.
- 1331 Plumb, R. A., & Ko, M. K. (1992). Interrelationships between mixing ratios of
 1332 long-lived stratospheric constituents. *Journal of Geophysical Research: Atmo-*
 1333 *spheres*, *97*(D9), 10145–10156.
- 1334 Plummer, D., Nagashima, T., Tilmes, S., Archibald, A., Chiodo, G., Fadnavis, S.,
 1335 ... others (2021). Ccmi-2022: A new set of chemistry-climate model initiative
 1336 (ccmi) community simulations to update the assessment of models and support
 1337 upcoming ozone assessment activities. *Newsletter n 57 July 2021*, 22.
- 1338 Polvani, L. M., Wang, L., Abalos, M., Butchart, N., Chipperfield, M. P., Dameris,
 1339 M., ... Stone, K. A. (2019). Large Impacts, Past and Future, of Ozone-
 1340 Depleting Substances on Brewer-Dobson Circulation Trends: A Multimodel
 1341 Assessment. *Journal of Geophysical Research: Atmospheres*, *124*(13), 6669-
 1342 6680. Retrieved from [https://agupubs.onlinelibrary.wiley.com/doi/abs/](https://agupubs.onlinelibrary.wiley.com/doi/abs/10.1029/2018JD029516)
 1343 [10.1029/2018JD029516](https://doi.org/10.1029/2018JD029516) doi: <https://doi.org/10.1029/2018JD029516>
- 1344 Prather, M. J., Hsu, J., DeLuca, N. M., Jackman, C. H., Oman, L. D., Douglass,
 1345 A. R., ... others (2015). Measuring and modeling the lifetime of nitrous ox-
 1346 ide including its variability. *Journal of Geophysical Research: Atmospheres*,
 1347 *120*(11), 5693–5705.
- 1348 Prignon, M., Chabrillat, S., Friedrich, M., Smale, D., Strahan, S., Bernath, P.,
 1349 ... others (2021). Stratospheric fluorine as a tracer of circulation changes:
 1350 comparison between infrared remote-sensing observations and simulations
 1351 with five modern reanalyses. *Journal of Geophysical Research: Atmospheres*,
 1352 e2021JD034995.
- 1353 Prignon, M., Chabrillat, S., Minganti, D., O’Doherty, S., Servais, C., Stiller, G., ...
 1354 Mahieu, E. (2019). Improved FTIR retrieval strategy for HCFC-22 (CHClF₂),
 1355 comparisons with in situ and satellite datasets with the support of models,
 1356 and determination of its long-term trend above Jungfraujoch. *Atmospheric*
 1357 *Chemistry and Physics Discussions*.
- 1358 Randel, W., Boville, B. A., Gille, J. C., Bailey, P. L., Massie, S. T., Kumer, J., ...
 1359 Roche, A. (1994). Simulation of stratospheric N₂O in the NCAR CCM2:
 1360 Comparison with CLAES data and global budget analyses. *Journal of the*
 1361 *atmospheric sciences*, *51*(20), 2834–2845.
- 1362 Randel, W., & Park, M. (2019). Diagnosing observed stratospheric water vapor re-
 1363 lationships to the cold point tropical tropopause. *Journal of Geophysical Re-*
 1364 *search: Atmospheres*, *124*(13), 7018–7033.

- 1365 Rodgers, C. D. (2000). *Inverse methods for atmospheric sounding: theory and prac-*
 1366 *tice* (Vol. 2). World scientific.
- 1367 Šácha, P., Eichinger, R., Garny, H., Pišoft, P., Dietmüller, S., de la Torre, L., ...
 1368 others (2019). Extratropical age of air trends and causative factors in cli-
 1369 mate projection simulations. *Atmospheric Chemistry and Physics*, 19(11),
 1370 7627–7647.
- 1371 Scaife, A., & James, I. (2000). Response of the stratosphere to interannual variabil-
 1372 ity of tropospheric planetary waves. *Quarterly Journal of the Royal Meteorolo-*
 1373 *gical Society*, 126(562), 275–297.
- 1374 Seinfeld, J. H., & Pandis, S. N. (2016). *Atmospheric chemistry and physics: from air*
 1375 *pollution to climate change*. John Wiley & Sons.
- 1376 Sheese, P. E., Walker, K. A., Boone, C. D., Bernath, P. F., Froidevaux, L., Funke,
 1377 B., ... von Clarmann, T. (2017). ACE-FTS ozone, water vapour, nitrous
 1378 oxide, nitric acid, and carbon monoxide profile comparisons with MIPAS and
 1379 MLS. *Journal of Quantitative Spectroscopy and Radiative Transfer*, 186,
 1380 63–80.
- 1381 Shepherd, T. G. (2007). Transport in the middle atmosphere. *Journal of the Meteo-*
 1382 *rological Society of Japan. Ser. II*, 85, 165–191.
- 1383 Shepherd, T. G. (2008). Dynamics, stratospheric ozone, and climate change.
 1384 *Atmosphere-Ocean*, 46(1), 117–138. Retrieved from [https://doi.org/](https://doi.org/10.3137/ao.460106)
 1385 [10.3137/ao.460106](https://doi.org/10.3137/ao.460106) doi: 10.3137/ao.460106
- 1386 Simmons, A., Soci, C., Nicolas, J., Bell, B., Berrisford, P., Dragani, R., ... others
 1387 (2020). *Global stratospheric temperature bias and other stratospheric aspects of*
 1388 *ERA5 and ERA5. 1*. European Centre for Medium Range Weather Forecasts.
- 1389 Stiller, G., Clarmann, T. v., Haenel, F., Funke, B., Glatthor, N., Grabowski, U., ...
 1390 others (2012). Observed temporal evolution of global mean age of stratospheric
 1391 air for the 2002 to 2010 period. *Atmospheric Chemistry and Physics*, 12(7),
 1392 3311–3331.
- 1393 Stiller, G., Fierli, F., Ploeger, F., Cagnazzo, C., Funke, B., Haenel, F. J., ... Clar-
 1394 mann, T. v. (2017). Shift of subtropical transport barriers explains observed
 1395 hemispheric asymmetry of decadal trends of age of air. *Atmospheric Chemistry*
 1396 *and Physics*, 17(18), 11177–11192.
- 1397 Strahan, S. E., Douglass, A., Stolarski, R., Akiyoshi, H., Bekki, S., Braesicke, P., ...
 1398 others (2011). Using transport diagnostics to understand chemistry climate
 1399 model ozone simulations. *Journal of Geophysical Research: Atmospheres*,
 1400 116(D17).
- 1401 Strahan, S. E., Smale, D., Douglass, A. R., Blumenstock, T., Hannigan, J. W., Hase,
 1402 F., ... others (2020). Observed hemispheric asymmetry in stratospheric
 1403 transport trends from 1994 to 2018. *Geophysical Research Letters*, 47(17),
 1404 e2020GL088567.
- 1405 Strong, K., Wolff, M. A., Kerzenmacher, T. E., Walker, K. A., Bernath, P. F.,
 1406 Blumenstock, T., ... Wood, S. (2008). Validation of ACE-FTS N₂O mea-
 1407 surements. *Atmospheric Chemistry and Physics*, 8(16), 4759–4786. Re-
 1408 trieved from <https://acp.copernicus.org/articles/8/4759/2008/> doi:
 1409 [10.5194/acp-8-4759-2008](https://doi.org/10.5194/acp-8-4759-2008)
- 1410 Tian, H., Xu, R., Canadell, J. G., Thompson, R. L., Winiwarter, W., Sunthar-
 1411 alingam, P., ... Yao, Y. (2020). A comprehensive quantification of
 1412 global nitrous oxide sources and sinks. *Nature*, 586(7828), 248–256. doi:
 1413 [10.1038/s41586-020-2780-0](https://doi.org/10.1038/s41586-020-2780-0)
- 1414 von Clarmann, T., & Grabowski, U. (2021). Direct inversion of circulation from
 1415 tracer measurements—Part 2: Sensitivity studies and model recovery tests. *At-*
 1416 *mospheric Chemistry and Physics*, 21(4), 2509–2526.
- 1417 Wargan, K., Orbe, C., Pawson, S., Ziemke, J. R., Oman, L. D., Olsen, M. A.,
 1418 ... Emma Knowland, K. (2018). Recent Decline in Extratropical
 1419 Lower Stratospheric Ozone Attributed to Circulation Changes. *Geo-*

- 1420 *physical Research Letters*, 45(10), 5166-5176. Retrieved from [https://](https://agupubs.onlinelibrary.wiley.com/doi/abs/10.1029/2018GL077406)
1421 agupubs.onlinelibrary.wiley.com/doi/abs/10.1029/2018GL077406 doi:
1422 <https://doi.org/10.1029/2018GL077406>
- 1423 Waugh, D., & Hall, T. (2002). Age of stratospheric air: Theory, observations, and
1424 models. *Reviews of Geophysics*, 40(4), 1-1.
- 1425 Wolter, K., & Timlin, M. S. (2011). El Niño/Southern Oscillation behaviour since
1426 1871 as diagnosed in an extended multivariate ENSO index (MEI. ext). *Inter-*
1427 *national Journal of Climatology*, 31(7), 1074-1087.
- 1428 Xian, T., & Homeyer, C. R. (2019). Global tropopause altitudes in radiosondes and
1429 reanalyses. *Atmospheric Chemistry and Physics*, 19(8), 5661-5678.
- 1430 Zander, R., Mahieu, E., Demoulin, P., Duchatelet, P., Roland, G., Servais, C.,
1431 ... Rinsland, C. (2008). Our changing atmosphere: Evidence based on
1432 long-term infrared solar observations at the jungfraujoch since 1950. *Sci-*
1433 *ence of The Total Environment*, 391(2), 184-195. Retrieved from [https://](https://www.sciencedirect.com/science/article/pii/S0048969707010789)
1434 www.sciencedirect.com/science/article/pii/S0048969707010789 (Re-
1435 search at Jungfraujoch - Contributions to the International conference in
1436 celebration of the 75th anniversary of the High Altitude Research Station
1437 Jungfraujoch at Interlaken, Switzerland (11-13 September, 2006)) doi:
1438 <https://doi.org/10.1016/j.scitotenv.2007.10.018>
- 1439 Zhou, M., Langerock, B., Wells, K. C., Millet, D. B., Vigouroux, C., Sha, M. K.,
1440 ... De Mazière, M. (2019). An intercomparison of total column-averaged
1441 nitrous oxide between ground-based FTIR TCCON and NDACC mea-
1442 surements at seven sites and comparisons with the GEOS-Chem model.
1443 *Atmospheric Measurement Techniques*, 12(2), 1393-1408. Retrieved
1444 from <https://amt.copernicus.org/articles/12/1393/2019/> doi:
1445 [10.5194/amt-12-1393-2019](https://doi.org/10.5194/amt-12-1393-2019)